ARTICLES
https://doi.org/10.1038/s41587-019-0207-y
nature biotechnology

Immuno-SABER enables highly multiplexed and amplified protein imaging in tissues

Sinem K. Saka[1,2,11*], Yu Wang[1,2,3,11*], Jocelyn Y. Kishi[1,2], Allen Zhu[1,2], Yitian Zeng[1,3], Wenxin Xie[1,3], Koray Kirli[4], Clarence Yapp[5,6], Marcelo Cicconet[5], Brian J. Beliveau[1,2,10], Sylvain W. Lapan[3], Siyuan Yin[1,3], Millicent Lin[1,3], Edward S. Boyden[7], Pascal S. Kaeser[8], German Pihan[9], George M. Church[1,3] and Peng Yin[1,2*]

Spatial mapping of proteins in tissues is hindered by limitations in multiplexing, sensitivity and throughput. Here we report immunostaining with signal amplification by exchange reaction (Immuno-SABER), which achieves highly multiplexed signal amplification via DNA-barcoded antibodies and orthogonal DNA concatemers generated by primer exchange reaction (PER). SABER offers independently programmable signal amplification without in situ enzymatic reactions, and intrinsic scalability to rapidly amplify and visualize a large number of targets when combined with fast exchange cycles of fluorescent imager strands. We demonstrate 5- to 180-fold signal amplification in diverse samples (cultured cells, cryosections, formalin-fixed paraffin-embedded sections and whole-mount tissues), as well as simultaneous signal amplification for ten different proteins using standard equipment and workflows. We also combined SABER with expansion microscopy to enable rapid, multiplexed super-resolution tissue imaging. Immuno-SABER presents an effective and accessible platform for multiplexed and amplified imaging of proteins with high sensitivity and throughput.

In situ protein imaging using immunofluorescence maps specific targets within their native environment. Accurate representation of cell type and state requires visualization of multiple markers. However, conventional methods offer limited multiplexing of targets (typically no more than five) owing to spectral overlap of fluorophores. Several recent methods achieve higher multiplexing, but often with decreased sensitivity, throughput or accessibility. Multiplexed ion beam imaging (MIBI)[1,2], imaging mass cytometry (IMC)[3] and multiplexed vibrational imaging[4] use specialized instruments to point-scan small fields (for example, ~2–5 min per 50 μm × 50 μm) and hence are exceedingly slow for large centimeter-scale tissue sections. Fluorescence methods utilizing sequential antibody staining (for example, MxIF[5], CycIF[6,7] and 4i[8]) offer high accessibility and relatively fast image acquisition, but require multiple slow cycles of primary antibody incubation (typically hours per cycle) and can take weeks to image tens of targets[5–7]. Alternatively, DNA-barcoding methods simultaneously apply ten or more antibodies, labeled with orthogonal DNA barcodes, followed by fast sequential barcode readout either through rapid binding and unbinding of fluorescent imager strands using DNA-Exchange (DEI)[9–11] or by in situ polymerization of fluorescent dNTP analogs (CODEX)[12], reducing experimental time to a couple of days. However, to overcome the overlap of antibody host species, high multiplexing requires conjugating DNA strands to primary antibodies, which results in lower signal (due to the lack of amplification from secondary antibodies) and decreased sensitivity, especially for low-abundance targets in tissues with high autofluorescence and scattering and low antigen access. Limited signal further lengthens the image acquisition times and reduces throughput. In situ signal amplification is thus needed to improve signal, throughput and sensitivity. The ideal amplification method should be scalable and compatible with rapid multiplexing, individually tunable for each target to accommodate the high dynamic range of the proteome[13], and applicable for spatially overlapping dense targets. However, existing methods do not satisfy these requirements.

Tyramide signal amplification (TSA)[14] amplifies the signal through covalent binding of diffusive tyramide molecules in the vicinity of the target. Owing to the lack of orthogonal chemistries, TSA amplifies one target per round, and necessitates slow rounds of (typically microwave-based) antibody removal for spectral multiplexing[15,16]. In contrast, by using orthogonal sequences, DNA-based methods allow simultaneous signal amplification. In rolling circle amplification (RCA)[17], a processive polymerase acts on a circular template to synthesize long concatenated repeats. RCA offers high levels of amplification and potential for multiplexing, but the in situ enzymatic reaction is hard to control or tune for individual targets[18]. TSA and RCA may also lead to blurring of signals and decreased resolution, respectively, owing to spreading of the tyramide molecules or the large size of the amplicons (reaching from 250 nm to over 1 μm in radius[19,20]). Branched DNA assemblies[21,22], such as RNAscope[23], generate complex tree structures for stable binding of fluorescent DNA strands, whereas the hybridization chain reaction (HCR) utilizes triggered assembly of metastable fluorophore-conjugated hairpins[24–26]. The structural complexity of existing

[1]Wyss Institute for Biologically Inspired Engineering, Harvard University, Boston, MA, USA. [2]Department of Systems Biology, Harvard Medical School, Boston, MA, USA. [3]Department of Genetics, Harvard Medical School, Boston, MA, USA. [4]Department of Biomedical Informatics, Harvard Medical School, Boston, MA, USA. [5]Image and Data Analysis Core, Harvard Medical School, Boston, MA, USA. [6]Laboratory of Systems Pharmacology, Harvard Medical School, Boston, MA, USA. [7]Media Lab, Massachusetts Institute of Technology (MIT), Cambridge, MA, USA. [8]Department of Neurobiology, Harvard Medical School, Boston, MA, USA. [9]Pathology Department, Beth Israel Deaconess Medical Center, Boston, MA, USA. [10]Present address: Department of Genome Sciences, University of Washington, Seattle, WA, USA. [11]These authors contributed equally: Sinem K. Saka, Yu Wang. *e-mail: sinem.saka@wyss.harvard.edu; yuwang01@fas.harvard.edu; py@hms.harvard.edu

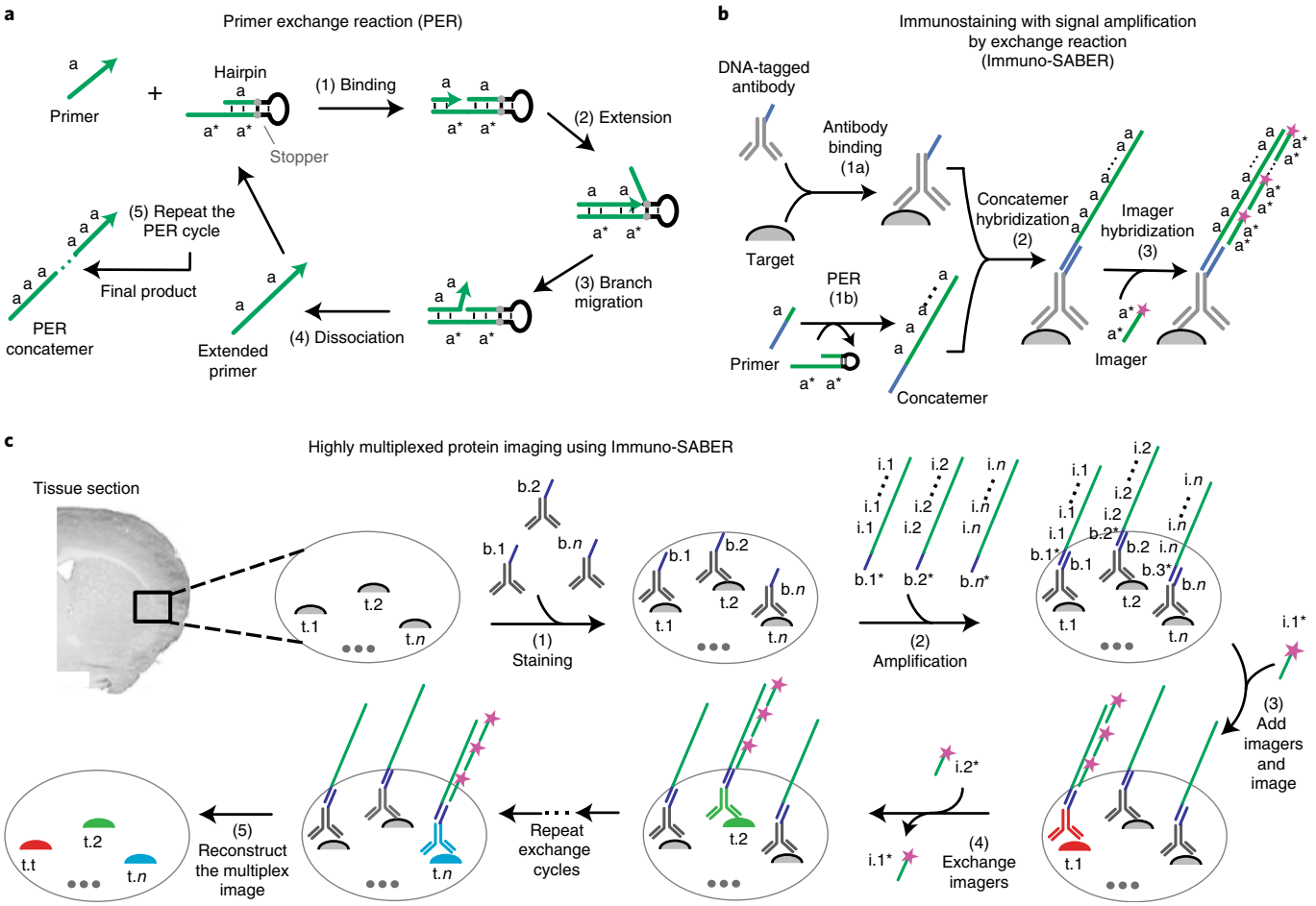

Fig. 1 | Immuno-SABER schematic. a, PER mechanism[29]. (1) A 9-nucleotide primer sequence *a* binds to the single-stranded *a** sequence on a hairpin (the asterisk indicates reverse complementarity). (2) The primer is extended by a strand-displacing polymerase (for example, Bst) isothermally and autonomously. The hairpin features a stopper sequence that halts polymerization, which releases the polymerase. (3) The newly synthesized *a* sequence is displaced from the hairpin through branch migration. (4) The extended primer and the hairpin autonomously dissociate. (5) Repetition of this copy-and-release process produces a long concatemer of *a*. **b**, Immuno-SABER schematic. (1a) Antibodies conjugated with bridge strands are used to simultaneously stain multiple targets. (1b) Primer sequences (green) are independently extended to a controlled length using PER. (2) Concatemers hybridize to the bridge sequence (blue) on the antibody. (3) Fluorophore (purple star)-labeled 20-nucleotide DNA imager strands hybridize to the repeated binding sites on the concatemers. Each imager is designed to bind to a dimer of the unit primer sequence. **c**, Exchange-SABER schematic. (1) Different biological targets (t.1 to t.*n*) are labeled with antibodies conjugated to orthogonal bridge strands (b.1 to b.*n*). (2) Orthogonal pre-extended concatemers are hybridized (via bridge complements b.1* to b.*n**) to the bridge strands on the antibodies simultaneously. (3) Target t.1 is visualized by hybridization of imager i.1* to the i.1 sites on the concatemer bound to b.1 on the corresponding antibody. (4) Multiple targets can be imaged sequentially by hybridization and dehybridization of orthogonal imagers in multiple rapid exchange cycles. (5) The images are computationally aligned and pseudocolored to overlay different targets.

DNA-assembly-based platforms could present potential challenges for designing highly multiplexed orthogonal systems. In practice, simultaneous signal amplification for proteins beyond spectral multiplexing (3–5 targets) has not been demonstrated[27,28].

Here we report Immuno-SABER, a highly multiplexed and individually controllable signal amplification method free of in situ enzymatic reactions (Fig. 1). After staining a sample with multiple DNA-barcoded primary antibodies, SABER involves hybridization of these barcodes to orthogonal single-stranded DNA concatemers, which are generated in a preprogrammed manner via primer exchange reactions (PERs)[29] (Fig. 1a) and bind multiple fluorophore-bearing imager strands for multiplexed signal amplification[30] (Fig. 1b). Rapid spectrally unlimited multiplexing can be achieved via Exchange-SABER, which combines SABER amplification with rapid exchange cycles of fluorescent imager strands[9–11] (Fig. 1c). We validated Immuno-SABER in diverse samples, including cultured cells, cryosections, formalin-fixed paraffin-embedded (FFPE) sections and whole-mount tissues, and demonstrated 5- to 180-fold signal amplification that was independently tunable, covering the range conventionally achieved by secondary antibodies to TSA. The simple design of SABER amplifiers makes it scalable. We further demonstrate simultaneous signal amplification and imaging of ten protein targets in tissues. Finally, we combine SABER with expansion microscopy (ExM)[31] to achieve rapid highly multiplexed super-resolution tissue imaging.

Results

Validation of in situ signal amplification by Immuno-SABER. For in situ signal amplification, Immuno-SABER relies on controlled in vitro synthesis of amplifier concatemers by PER, followed by programmed in situ assembly. PER utilizes a catalytic hairpin for controlled extension of a short primer sequence in an iterative manner (as in Fig. 1a). Primer designs rely on a three-letter code (made of only A, T and C nucleotides), where G nucleotides are avoided in

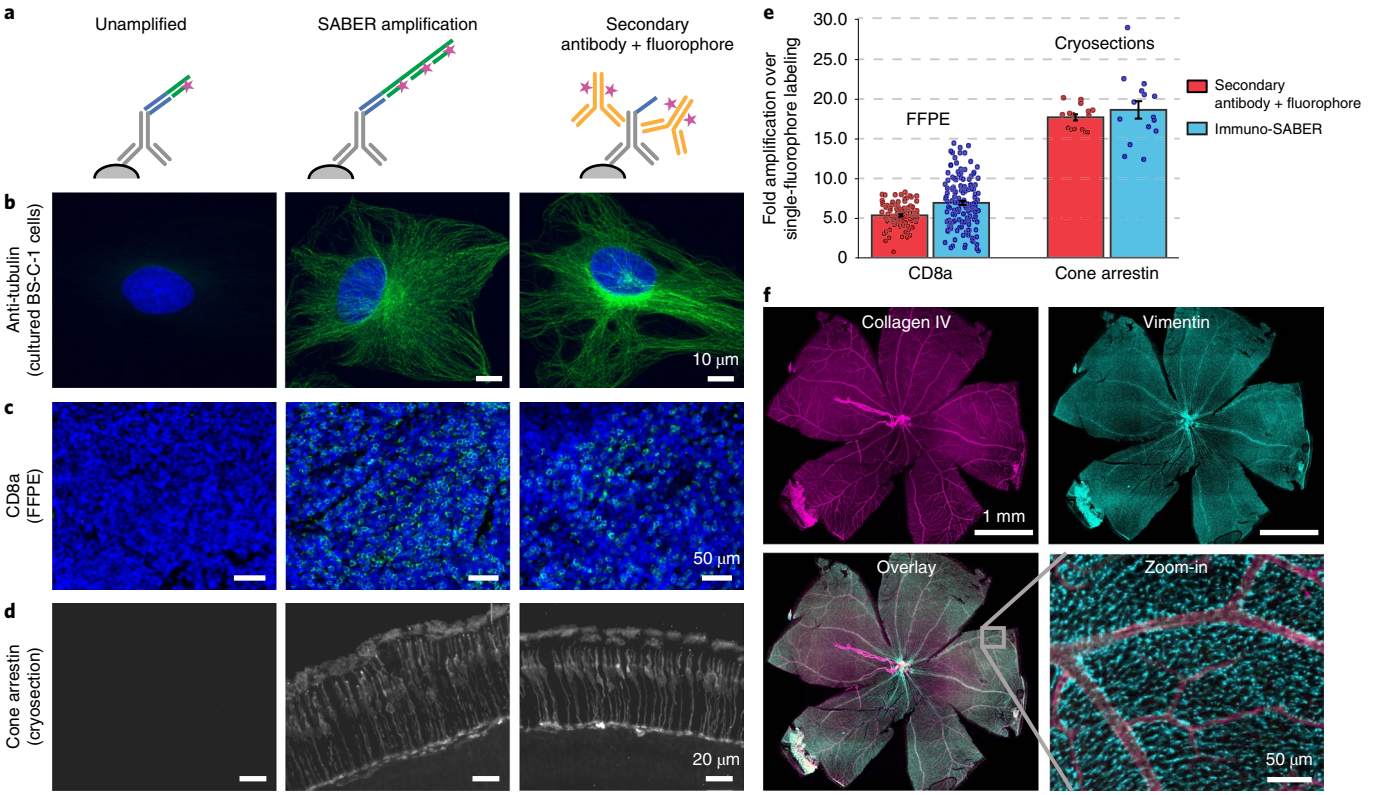

Fig. 2 | Validation and quantification of signal amplification by Immuno-SABER. a, Cultured BS-C-1 cells were immunostained for α-tubulin and the following three conditions were prepared for comparison: an unamplified condition, in which unextended primers with a single binding site for the imager (with Alexa Fluor 647) were hybridized to the bridge on the antibody; an amplified condition, in which the extended concatemer was hybridized for signal amplification (linear amplification); and a control condition, in which conventional antibody staining was performed with Alexa Fluor 647-conjugated secondary antibodies. **b**, Representative images of each condition from **a** (maximum projections from the confocal *z* stack taken with a 63× objective). **c**, Representative images for CD8a staining (labeled with an Atto488 imager) in human tonsil FFPE sections (single-plane large-area scans with a 20× objective cropped to show a region of the interfollicular zone that is rich in $CD8^+$ cells). **d**, Cone arrestin staining in mouse retina cryosections (maximum projection of a confocal *z* stack taken with a 20× objective). See the Methods for experimental details. **e**, The level of signal amplification by Immuno-SABER was quantified by measuring the background-subtracted mean fluorescence for several ROIs in the tissues and is expressed as the fold signal amplification over the unamplified signal level. Conventional secondary antibody amplification was also quantified similarly and is shown as reference. For CD8a FFPE sections, $n = 80$ (for unamplified), $n = 100$ (for SABER) and $n = 94$ (for conventional) rectangular ROIs (each covering 0.03–1.20 mm^2 tissue regions; consecutive tissue sections are used for the three conditions). For cone arrestin, $n = 6$ images were taken from two retina samples. Error bars, s.e.m. **f**, Immuno-SABER was performed in whole-mount retina sections for collagen IV and vimentin. Maximum projections from confocal *z* stacks are displayed.

the primer sequence and in the reaction mixture[29,30]. Hence, the C nucleotide after the template on the hairpin acts as a stopper for the polymerase. This simple step-by-step synthesis offers tight control of the reaction by external parameters (such as hairpin or dNTP concentration, reaction time and temperature) as well as high programmability and yields long DNA concatemers of desired lengths reaching >500 nucleotides[30]. For a modular design, we conjugated antibodies with 42-nucleotide DNA sequences ('bridges'; from the orthogonal library we designed previously[30]), which enable hybridization of concatemers through their 5′ sections of sequence that are complementary to the bridges. To preserve antigen recognition, we optimized our protocol to conjugate 1–3 oligonucleotides per antibody (see Supplementary Note 1). We also developed an optional purification strategy based on toehold displacement-mediated DNA affinity pull-down (Supplementary Fig. 1).

For application of our in vitro extension and in situ assembly strategy on biological specimens, labeling specificity, resolution and amplification efficiency are the main considerations. First, to evaluate the specificity and preservation of morphology, we performed Immuno-SABER staining of microtubules in cultured cells as a test case for a densely arranged structural protein target. We observed specific staining, clear tubular morphology and a similar staining pattern to conventional immunostaining with fluorophore-conjugated secondary antibodies (Fig. 2a,b). The resolution of the images, as quantified by the full-width-half-maximum (FWHM) of the fitted line plots across the thin microtubules, was unaltered as compared to the secondary antibody control (Supplementary Fig. 2a–c). These results demonstrated the suitability of Immuno-SABER for in situ labeling of proteins, with high resolution and high specificity even in dense arrangements.

For validation of the labeling strategy in tissue samples and quantification of the signal amplification, we used the following two types of tissue preparations: 5-μm-thick FFPE human tonsil sections and 40-μm-thick mouse retina cryosections. Both tissue types provide a good validation platform owing to the morphologically distinct and well-conserved organization of different cell types that can be identified by well-established biomarkers. The retina has a layered organization of different types of cells whereas tonsils feature multiple germinal centers with stereotypic organization of a large number of distinct cell types.

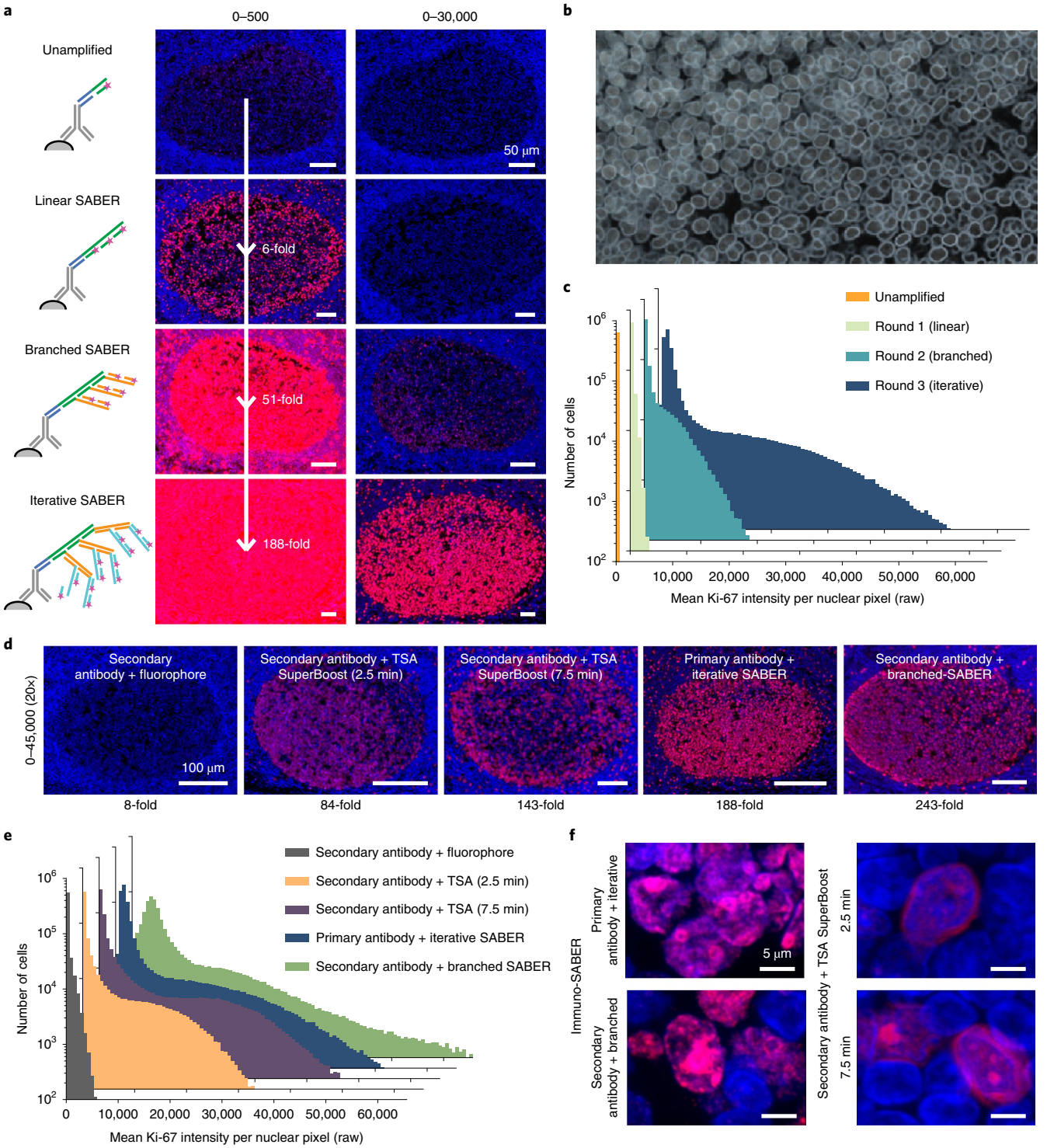

Fig. 3 | Immuno-SABER signal can be further amplified through branching. a, Nuclear Ki-67 (Alexa Fluor 647, red) imaging with DAPI (blue) in the Ki-67-rich germinal center of FFPE human tonsil sections shown after up to three rounds of amplification (iterative SABER). Sixteen-bit images were scaled to two different maximum pixel values (500 and 30,000) to allow visual comparison. Signals were quantified in each case versus the unamplified sample and the fold changes are provided. **b**, Machine-learning-based contouring of the nuclei for quantification of signal per cell. See Supplementary Fig. 5a and the Methods for more information. **c**, Mean Ki-67 signal intensity for each nucleus was obtained from automated segmentation and the histogram was plotted for the whole tissue section for each condition. The consecutive sections each contain 636,479–717,176 identified nuclei. **d**, Images show germinal centers in FFPE human tonsil sections with Ki-67 labeling (red) with conventional secondary antibody–fluorophore staining, TSA (with HRP-conjugated secondary antibodies) for 2.5 and 7.5 min, primary antibodies using iterative SABER amplification or secondary antibodies using branched SABER amplification. TSA was applied using poly(HRP)conjugated secondary antibodies from a commercial SuperBoost Kit with 2.5 or 7.5 min of incubation with tyramide–Alexa Fluor 647. The amplification levels are noted below the images. **e**, Histograms to visualize mean nuclear signal level were plotted for the conditions in **d**. The consecutive tissue sections each contain 586,183–717,176 cells. **f**, Samples were imaged with a confocal microscope at a higher resolution with 63× magnification to evaluate signal blurring. Images with different scaling are displayed in Supplementary Fig. 5f.

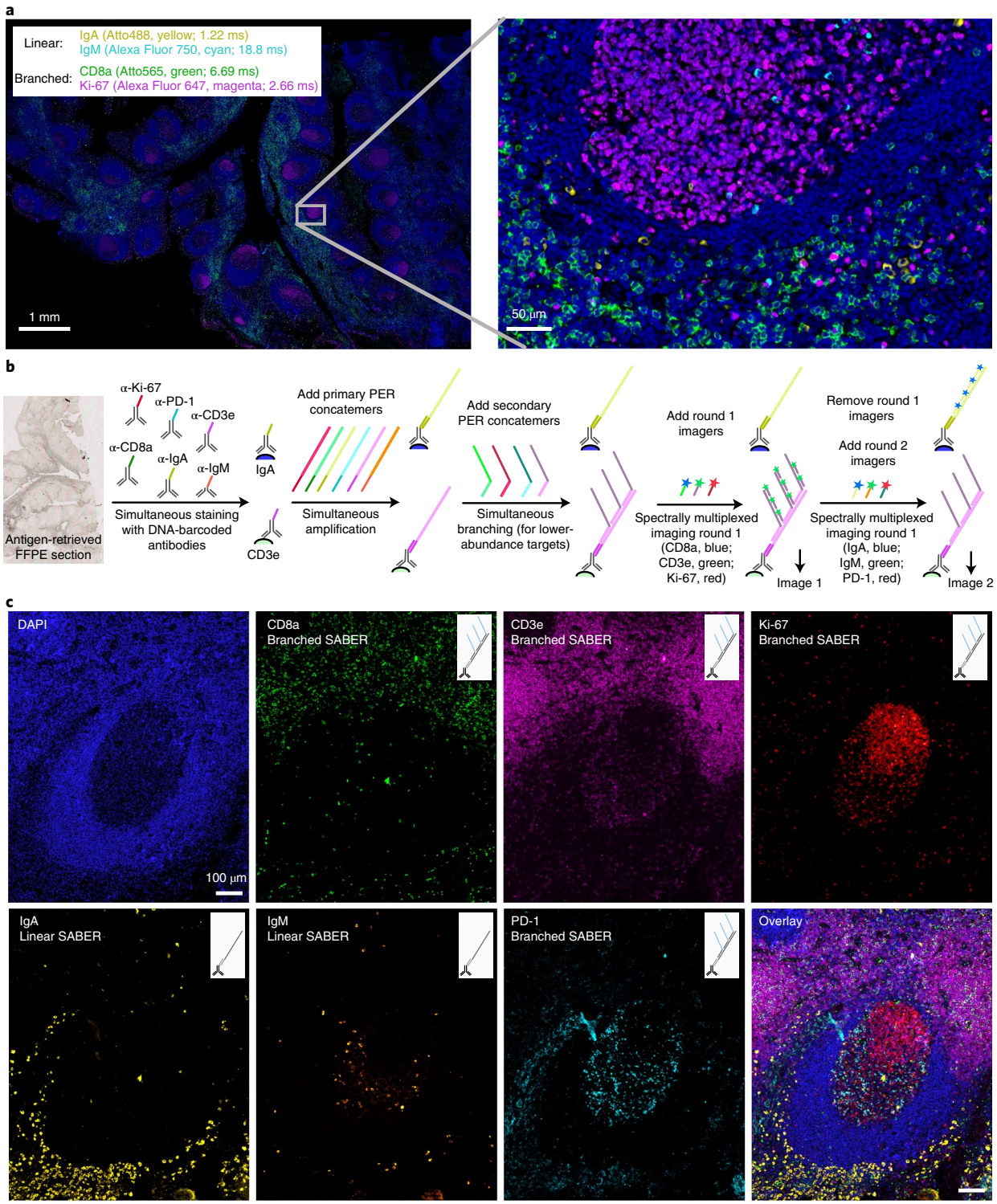

Fig. 4 | Immuno-SABER and Exchange-SABER in FFPE human tonsil samples. a, Left, centimeter-scale whole-slide imaging of human tonsil sections with five-color spectral multiplexing (DAPI and four other targets). Right, an expanded view of the region marked with the gray box showing four-target imaging with subcellular resolution with a ×20 objective. Exposure times for each target (autoexposure setting) are indicated in a white box. For IgA and IgM (higher copy number), linear amplification yields high enough signal to achieve autoexposure times of 1–20 ms under optimized conditions. For Ki-67 and CD8a (lower copy number)[47,48], branched amplification (one round of branching) was applied to allow auto-exposure times of 2–10 ms. **b**, Higher multiplexing via Exchange-SABER. The schematic for the multiplexed imaging workflow where all antibodies were applied simultaneously, followed by simultaneous amplification and sequential rounds of imaging. IgA and CD3e labeling structures are shown as examples to illustrate the workflow for linear and branched SABER on the same sample. **c**, Images show an expanded view of a germinal center in human FFPE tonsil sections imaged in seven colors (DAPI and six other targets) with a single exchange round (round 1, top row; round 2, bottom row). Four of the targets, CD8a (Atto488), CD3e (Alexa Fluor 647), Ki-67 (Alexa Fluor 750) and PD-1 (Alexa Fluor 750), were visualized with simultaneous branched SABER amplification, whereas IgA (Atto488) and IgM (Atto565) were visualized with linear amplification.

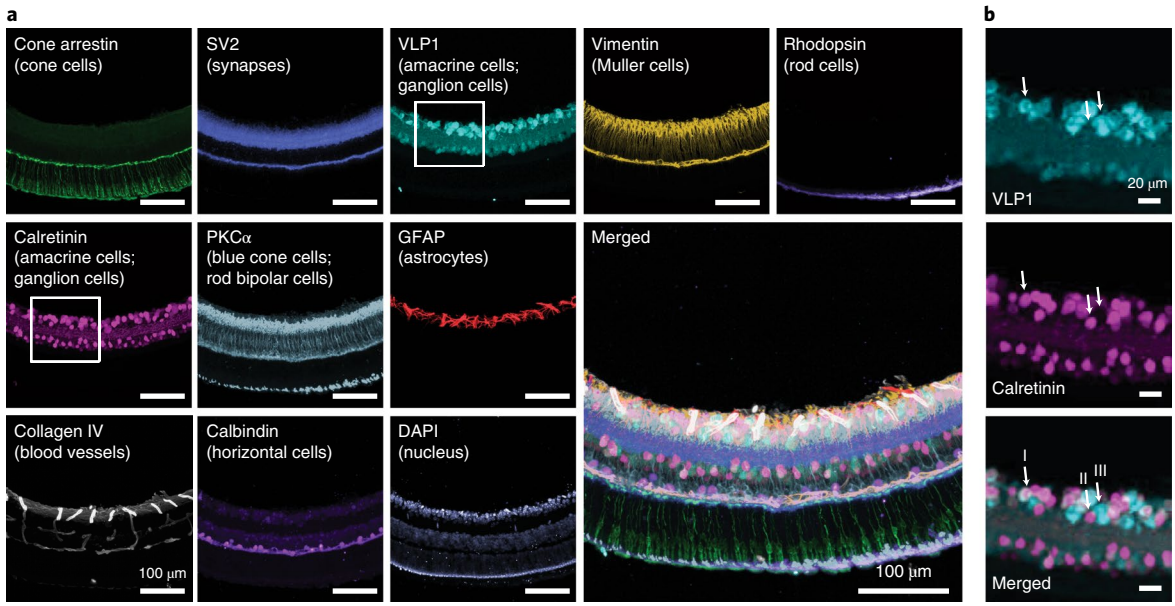

Fig. 5 | Exchange-SABER in mouse retina cryosections. a, Ten protein targets labeling various retinal cell types were visualized in 40-µm-thick mouse retina cryosections. The markers targeted with Immuno-SABER were rhodopsin (rod photoreceptors), GFAP (astrocytes), vimentin (Muller cells[9]), collagen IV (blood vessels), three calcium-binding proteins[49,50] (VLP1, calretinin (found in a subset of amacrine and ganglion cells) and calbindin (note that, although calbindin was suggested to be also found in a subset of amacrine and ganglion cells, the anti-calbindin antibody used here mostly labels horizontal cells[50])) and PKCα (blue cone cells and rod bipolar cells[50]). The sections were first incubated with all of the DNA-conjugated antibodies simultaneously. All SABER concatemers were then added simultaneously to the sample, followed by washing and sequential incorporation of the imager strands and multiround imaging. A *z* stack of images was acquired for each target, and DAPI was imaged in every exchange cycle to monitor sample drift. The maximum projected images of each stack were computationally aligned using a subpixel registration algorithm with DAPI as the drift marker[9], and pseudocolored for the overlay presentation. **b**, Expanded view of the area marked by the white rectangle in **a**. Three cell subtypes (marked with arrows: I, VLP1$^+$ and calretinin$^+$; II, VLP1$^-$ and calretinin$^+$; III, VLP1$^+$ and calretinin$^-$) can be differentiated on the basis of VLP1 and calretinin expression.

For the FFPE samples, we imaged the T cell membrane marker CD8a. CD8a$^+$ cells are largely present in the marginal zone (outside of germinal centers)[32]. For mouse retina cryosections, we imaged cone arrestin, a specific marker of cone photoreceptor cells[9]. Both markers showed signal patterns consistent with the expected distribution of the markers, suggesting high specificity (Fig. 2c,d). For both targets and sample types, Immuno-SABER yielded similar or slightly higher fluorescence signal than conventional fluorophore-conjugated secondary antibody staining using the same fluorophore. We quantified the signal amplification level as 6.7-fold for CD8a and 19.4-fold for cone arrestin. For comparison, conventional secondary antibody staining yielded 5.3- and 17.5-fold signal amplification, respectively (Fig. 2e). Overall, our strategy generated an improvement of approximately 5- to 20-fold in the signal level as compared to the unamplified control, reaching amplification in the range of secondary antibodies. The degree of in situ signal amplification may depend on multiple factors, including the abundance and organization of targets, the antibodies (for example, clonality and conjugation efficiency) and the method of quantification (the unamplified signal level, thresholding and background subtraction), as well as the experimental conditions and properties of the SABER sequences (for example, concatemer length[30]).

Despite reaching >500 nucleotides in length, SABER concatemers can effectively penetrate relatively thick samples. We validated the concatemer penetration capability in whole-mount preparations of mouse retina by successfully staining for the Muller cell marker vimentin and the blood vessel marker collagen IV, which were both predominantly detected in the 100-µm region between the nerve fiber layer and the outer plexiform layer of the retina, as expected[33] (Fig. 2f and Supplementary Fig. 2d). This high penetration may potentially be attributed to SABER concatemers being largely linear DNA structures that are designed using a three-letter code to minimize secondary structures.

Enhancement of signal through branching. To enable further signal enhancement, which would increase the sensitivity for the proteins of lower abundance or improve imaging throughput, we developed a sequential amplification strategy where independently extended secondary concatemers can be branched off the primary concatemer to create more binding sites for fluorescent imagers (branched SABER; Supplementary Fig. 3a). We performed similar tests to check the effect of an additional amplification round targeting the same proteins in cell culture, human FFPE tonsil tissues and mouse retina cryosections (Supplementary Fig. 3b,c). With one round of branching, we obtained an additional 2.8-fold signal amplification for CD8a in FFPE sections and a 8.4-fold signal amplification for cone arrestin in cryosections as compared to a single round (Supplementary Fig. 3d). Microtubule staining in cells indicates that the specificity of labeling and the high-resolution morphology of the target were still preserved with branched SABER (Supplementary Fig. 3e). FWHM estimations demonstrated that the sizes of the structures were still bound by the diffraction-limit and were not significantly altered (Supplementary Fig. 3f).

To evaluate the preservation of access to the target and variation in overall signal distribution, we performed baseline quantification and linear and branched amplification for a ubiquitous protein (lamin B) in the same sample of HeLa cells using DNA-conjugated secondary antibodies and varying lengths of concatemers and branches (Supplementary Fig. 4). We did not detect a significant difference in the baseline signal for concatemers up to 700 nucleotides in length (for linear amplification), suggesting that the length range we utilized in our experiments did not cause decreased

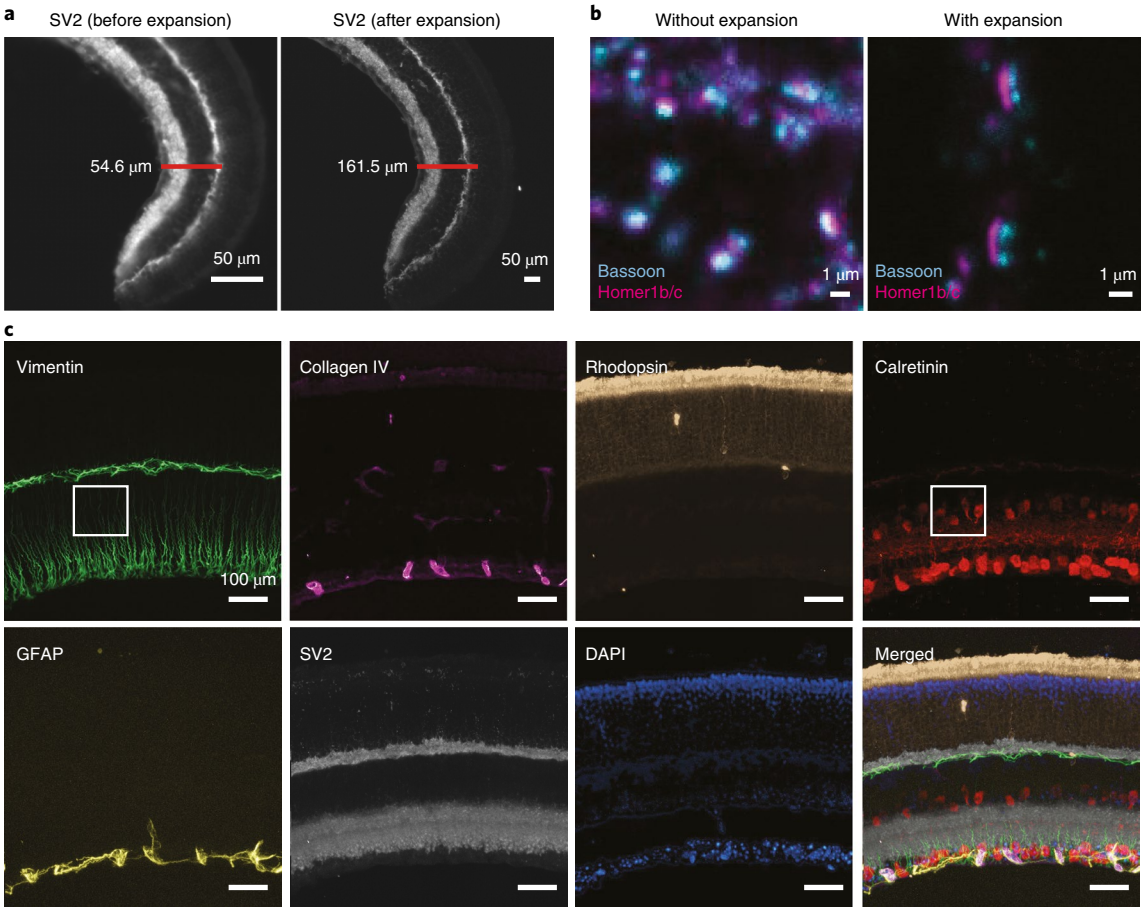

Fig. 6 | Multiplexed super-resolution imaging using Expansion-SABER. a, Forty-micrometer-thick mouse retina cryosections were stained for SV2 using DNA-conjugated anti-SV2 antibodies, followed by SABER concatemer hybridization. Images were acquired before hydrogel formation and after hydrogel formation and expansion (approximately threefold) using the original expansion protocol[31,39]. **b**, Images of pre- and postsynaptic sites of neuronal synapses in fixed primary mouse hippocampal neuron culture samples with and without expansion (different fields of view are shown). The presynaptic sites were labeled with anti-Bassoon antibodies and the post-synaptic sites were labeled with anti-Homer1b/c antibodies. DNA-conjugated secondary antibodies were used to target anti-Bassoon and anti-Homer1b/c primary antibodies, and SABER concatemers were then applied. **c**, ExM imaging of six protein targets in the originally 40-μm-thick mouse retina section (expanded approximately threefold) with Exchange-SABER. Two exchange rounds with Atto488-, Atto565- and Alexa Fluor 647-conjugated imager strands were performed to visualize all six targets in the expanded samples. DAPI was imaged in both rounds to serve as a registration marker. The images are maximum projections of *z* stacks, drift corrected using DAPI channels and pseudocolored for presentation. An expanded view of the boxed region is available in Supplementary Fig. 9b.

access (Supplementary Fig. 4b,g). For reference, we also compared the baseline signal to the signal from secondary antibodies, which, on average, were conjugated to five fluorophores. We were able to see that in this case signal level was approximately fivefold higher than the single-fluorophore baseline, further demonstrating comparable antigen access (Supplementary Fig. 4c). For the increasing concatemer lengths, the expected amplification trend was obtained across samples with quantitatively consistent intensity values. Blue bars in Supplementary Fig. 4b,g can be compared for more insights; for example, for linear amplification, approximately twofold higher signal intensities were obtained with the long primary concatemers (700 nucleotides) versus the short primary concatemers (350 nucleotides).

Immuno-SABER allows further improvement of sensitivity by performing multiple branching rounds (iterative SABER). We applied this strategy both in tonsil FFPE sections and mouse retina cryosections, and performed three sequential amplification rounds following primary antibody staining. We targeted the proliferating cell nuclear marker Ki-67 that is mainly found in the germinal center (that is, the dark zone) in tonsil sections and the synaptic marker SV2 that is found mainly in synapses of both the outer and inner plexiform layers[9]. Figure 3a shows Ki-67-rich germinal centers stained at different amplification levels, displayed at two different contrast scales to allow visual comparison of the signal.

To follow the change in the signal level for individual nuclei in the whole-section scans, we developed a machine learning algorithm that automatically annotates DAPI-defined nuclear contours (Fig. 3b and Supplementary Fig. 5a) for nuclear segmentation. This allowed us to assign mean Ki-67 signal intensity to individual nuclei in sections of 550,000–750,000 cells each, and plot histograms for each amplification condition (Fig. 3c). The total nuclear signal for each condition gave a basic quantitative estimate of the amplification level with respect to the unamplified case, yielding 6-, 51- and 188-fold signal amplification, respectively for linear, branched and iterative SABER (Fig. 3a). Although the amplification process is exponential in nature, throughout the three rounds the coefficient of variation (s.d. over the mean) for the population remained at a similar level (round 1 = 1.76; round 2 = 1.65; round 3 = 1.55), suggesting that increased amplification level does not create a substantial variation in the distribution.

For these samples, concatemer hybridizations can also be performed for shorter durations (for example, with incubation times down to 75 min per round (instead of overnight for the longer primary concatemer, and 3 h for branching as in Fig. 3a) without significant difference in signal level (Supplementary Fig. 5b,c). Iterative SABER (three rounds) was also applied for SV2 in thicker mouse retina cryosections, generating ~80-fold signal amplification (Supplementary Fig. 5d).

For such high levels of amplification, catalyzed reporter-deposition-based TSA is considered a gold standard, with reports of 10- to 1,000-fold signal amplification[14,34,35]. This can be further improved 2- to 10-fold via poly-horseradish peroxidase (HRP)-conjugated secondary antibodies. However, TSA is not suitable for simultaneous multiplexed amplification owing to the lack of orthogonal chemistries and difficulty in controlling the in situ reaction, and is also not ideal for high-resolution imaging owing to spreading of the fluorescent tyramide molecules, which causes blurring[20]. To investigate how Immuno-SABER performs in comparison, we first utilized a commercial kit for conventional TSA with mono-HRP-conjugated secondary antibodies and Alexa Fluor 647–tyramide. In retina cryosections, we observed that iterative SABER (with conjugated primary antibodies) could amplify the signal to a higher level than TSA with secondary antibodies (Supplementary Fig. 5e). We also used the commercial SuperBoost kit that features poly-HRP-conjugated secondary antibodies for Ki-67 staining of FFPE tonsil sections, which yielded up to 143-fold signal amplification (Fig. 3d,e), Comparatively, both iterative SABER (188-fold; Fig. 3a) with primary antibodies and branched SABER (two rounds) using secondary antibodies (243-fold) yielded higher signal than TSA (Fig. 3d,e). Where species overlap is not of concern (single or low-plex imaging), linear or branched SABER with secondary antibodies can be performed for increased signal with better-preserved morphology.

At this high amplification level, Immuno-SABER still provided crisp staining and preserved the subcellular morphology, whereas TSA staining resulted in blurring of the signal and spilling over of the label from the target compartments (Ki-67 is a nuclear protein that is highly enriched in nucleoli), as signal coming from outside of DAPI-labeled nuclei could be observed in the high-magnification confocal images (Fig. 3f and Supplementary Fig. 5f,g). Increasing the tyramide incubation period to 10 min (2–10 min being the manufacturer-recommended optimization range) worsened the blurring (Supplementary Fig. 5f,g).

Simultaneous multiplexed amplification by Immuno-SABER. Outside of a preference for single-stranded concatemers that is facilitated by the use of a three-letter code, PER has few inherent restrictions in sequence design, making design of orthogonal sequences straightforward. We previously developed a computational pipeline to design orthogonal PER primer–hairpin pairs with maximum extension efficiency and minimum crosstalk by utilizing in silico simulations using NUPACK[36] and designed 50 orthogonal sequences to enable multiplexed imaging[29,30]. Here we tested 32 primer sequences and extended each into long DNA concatemers in a controlled fashion up to the target length range of 600–700 nucleotides (Supplementary Fig. 6a). As extension efficiency is sequence dependent, reaction conditions were optimized for each primer by modulating the hairpin concentration and reaction time to obtain concatemers of similar length (Supplementary Table 1). All of the tested primers extended into long concatemers in the desired length range, with 31 of 32 sequences (except sequence 51) yielding a predominant long concatemer band, albeit with some heterogeneity in the distribution of shorter reaction products (Supplementary Fig. 6a). Next, we evaluated the orthogonality of detection (crosstalk check) in situ through an imaging-based multiwell plate assay. We targeted α-tubulin with DNA-conjugated antibodies in cells, and applied each concatemer in separate wells with its cognate imagers or with all other imagers. All 32 sequences yielded specific staining, and we observed minimal crosstalk (crosstalk signal/cognate signal = 4%) for only one non-cognate imager–primer pair (Supplementary Fig. 6b–e), suggesting that all other sequence combinations are suitable for multiplexed detection.

Next, we sought to validate the applicability of Immuno-SABER for independently programmed multiplexed signal amplification in tissues. We first tested spectral multiplexing on 5-µm-thick human FFPE tonsil sections. FFPE samples are the standard preparations for clinical settings and for archival purposes. However, these preparations suffer from autofluorescence and low antigen access, making amplification of the target signal a necessity. Clinical immunohistochemistry procedures typically utilize amplification methods such as chromogenic reactions to improve sensitivity, limiting the multiplexing capability to only one target per section. Multiple thin sections have to be prepared to stain different markers, which is not ideal as biopsy-based sample collection is invasive and samples can be scarce. Imaging throughput is another big concern, as typically centimeter-scale tissues need to be imaged by whole-slide scanning.

After standard preparation protocols for deparaffinization and antigen retrieval, we simultaneously stained the samples for Ki-67, CD8a, IgA and IgM using antibodies conjugated to orthogonal bridge sequences. Among these targets, IgA and IgM are expressed at high levels, whereas Ki-67 and CD8a are more moderately expressed (as a proxy, in the tonsil tissue, the RNA expression level of IgJ, the joining chain domain for multimeric IgA and IgM, was found to be 1,360 tags per million (TPM), while Ki-67 and CD8a expression was 15 and 19 TPM, respectively[37]). We performed whole-slide scanning with five-color spectral multiplexing (DAPI and four other targets) (Fig. 4a). Immuno-SABER amplification also enables improved imaging throughput by allowing short exposure times. For the abundant proteins IgA and IgM, linear amplification provided bright enough signal to permit 1–20 ms exposure times at 20× magnification. For moderately available proteins (Ki-67 and CD8a), branched SABER enabled 2–10 ms camera exposures and fast high-quality scans at subcellular resolution (Fig. 4a).

Next, we utilized Exchange-SABER to increase the multiplexing level and image different cell types in germinal centers with six markers (CD8a, CD3e, Ki-67, PD-1, IgA and IgM) (Fig. 4b). SABER amplification was applied simultaneously for all targets via hybridization of concatemers to the orthogonal bridge strands on the antibodies. Simultaneous branching was applied to the four less abundant targets (CD3e, CD8a, Ki-67 and PD-1) following primary concatemer hybridization, and three markers were imaged per round in two rounds as depicted in Fig. 4b. Figure 4c shows a germinal center with interfollicular zone. With our exchange protocol, efficient imager removal can be performed in 10 min without displacing the concatemers (Supplementary Fig. 7).

Exchange-SABER imaging in mouse retina cryosections. Next, we validated Immuno-SABER in 40-µm-thick cryosections and demonstrated ten-target protein imaging in mouse retina (Fig. 5). We first screened antibodies against a list of targets that have defined staining patterns, including cone arrestin, SV2, visinin-like protein 1 (VLP1), rhodopsin, calretinin, protein kinase C alpha (PKCα), glial fibrillary acidic protein (GFAP), vimentin, collagen IV and calbindin. We then conjugated DNA bridge strands to those antibodies, and validated the specificity and affinity of DNA-conjugated antibodies by comparing the staining patterns from conventional staining using unmodified primary antibodies followed by indirect immunofluorescence (Supplementary Fig. 8a). As controls for exchange imaging, we compared the pre- and post-washing images for SV2, and found the imager strands were efficiently removed after washing (Supplementary Fig. 8b) without sample damage or

signal loss (correlation coefficient between images >0.95 in three wash rounds (Supplementary Fig. 8c)).

The multiplexed imaging result showed that all targets were successfully captured with expected staining patterns (Fig. 5a). Interestingly, we found that two calcium-binding proteins, VLP1 and calretinin, together identify three populations of cells, VLP1^{+}calretinin^{-}, VLP1^{-}calretinin^{+} and VLP1^{+}calretinin^{+} cells (Fig. 5b). This observation was confirmed by validating the antibody specificity through comparing the staining patterns of three different antibodies against the same targets and by conventional indirect immunofluorescence using unconjugated primary antibodies (Supplementary Fig. 8d–f).

Fast multiplexed super-resolution imaging by Expansion-SABER. The spatial resolution of conventional fluorescence microscopy is limited by the diffraction of light. A variety of super-resolution techniques have been developed to overcome this limitation. Expansion microscopy (ExM), which improves the practical resolution by physically expanding hydrogel-embedded samples, enables subdiffraction imaging of tissues without specialized super-resolution instruments[31]. However, one challenge for ExM is the dilution of fluorescence signals during physical expansion, which creates a need for signal amplification. Both indirect immunofluorescence and HCR have been used to achieve higher signals in ExM with limited multiplexing capability[28]. A technique termed magnified analysis of the proteome (MAP) was developed to achieve higher multiplexing by combining expansion with repeated antibody staining and retrieval, demonstrating seven rounds of sequential labeling; however, owing to the slow permeation of the antibodies into the thick expanded tissue samples, each round of primary and secondary antibody staining takes 2–9 d, making the approach slow and laborious for higher levels of multiplexing[38].

To solve this problem, we combined ExM with SABER (Expansion-SABER). We modified the 5′ end of the SABER concatemers with an acrydite moiety that could be incorporated into polyacrylate hydrogels. Using the original ExM protocol[31] with Immuno-SABER for SV2 in mouse retina cryosections, we obtained approximately threefold expansion (Fig. 6a), which is slightly lower than the expansion factor reported before (~4.5-fold) owing to the shrinkage of the gel in the ionic gel re-embedding solution or in the imaging buffer with 0.5× PBS (as was also observed for the expansion-FISH protocol[31,39]). Higher levels of expansion can be attained by more recent expansion protocols that can achieve 10- to 20-fold expansion[40,41]. To validate the subdiffraction resolution, we imaged the presynaptic marker Bassoon and the post-synaptic marker Homer1b/c (which are typically ~160 nm apart[42]) in fixed primary mouse hippocampal neuron culture (Fig. 6b and Supplementary Fig. 9a). While Bassoon and Homer1b/c were readily separated after expansion, they strongly overlapped without expansion. We next demonstrated Exchange-SABER in expansion samples by visualizing six targets (vimentin, collagen IV, rhodopsin, calretinin, GFAP and SV2) in mouse retina cryosections (Fig. 6c). Individual Muller cells labeled by vimentin became clearly distinguishable after expansion (Supplementary Fig. 9b). As the expansion gel samples reached ~350 µm in thickness, we increased both the incubation time and wash time for imagers (to 45 min and 1.5 h, respectively) to achieve optimal imaging quality. We were able to perform six-target imaging in two rounds of imager exchange in 6 h—substantially faster than the MAP protocol, which would take >3 d (ref. [38]). To further increase the speed, we incorporated an alternative fluorophore removal protocol using imager strands with a disulfide bond between the DNA sequence and the fluorophore, which allow quick removal of the fluorescence signal by reducing agents (for example, TCEP)[43]. This approach shortened the signal removal time from 1.5 h to only 10 min (Supplementary Fig. 9c,d).

Discussion

Immuno-SABER provides a new highly multiplexed amplification capability to increase the detection sensitivity and tune it independently for multiple targets. To validate its suitability for tissue imaging, we addressed three main considerations. (1) Specific labeling of targets in commonly used sample preparations. We used SABER to label various protein targets (nuclear, cytoplasmic and membrane) in cell and tissue preparations (FFPE sections, cryosections and expansion samples), and reproduced the expected labeling patterns (Figs. 2, 4, 5 and 6 and Supplementary Figs. 2, 3 and 8). (2) Efficient access to the target and quantifiable amplification without sacrificing resolution. SABER probes can penetrate into whole-mount preparations and reach targets at depths of up to 100 µm (Fig. 2 and Supplementary Fig. 2). Linear amplification with primary antibodies in tissues yielded 5- to 20-fold signal enhancement (typically at a similar level to indirect immunofluorescence for the same target) (Figs. 2 and 3 and Supplementary Fig. 4). Branched SABER generated ~50-fold signal amplification (>5-fold higher signal than indirect immunofluorescence) and iterative SABER produced over 180-fold signal amplification (surpassing TSA) (Fig. 3 and Supplementary Fig. 5). At these levels of amplification, SABER did not have a significant impact on the resolution for conventional microscopy and tissue imaging (Fig. 2 and Supplementary Figs. 2 and 3). This observation still holds for super-resolution imaging with ExM (Fig. 6 and Supplementary Fig. 9). We also validated that the signal level can be further controlled by concatemer length and the concatemers (<700 nucleotides for linear and <450 nucleotides for branching) do not hinder access to antigens (Supplementary Fig. 4). (3) Multiplexing, through the use of orthogonal concatemers, we showed multiplexed amplification for ten protein targets in the same sample (Fig. 5) and simultaneous use of linear and branched SABER (Fig. 4). The ability to program and control the fold amplification of signal for each target is valuable for multiplexed imaging of target proteins expressed with a high dynamic range. To lead the way toward higher multiplexing, we performed in situ testing of a pool of 32 sequences from our 50 in silico-designed sequences[30], and detected minimal crosstalk for only 1 of the 1,024 pairs (Supplementary Fig. 6). Owing to the simplicity of sequence design, it is straightforward to upscale the orthogonal pool size and reach much higher multiplexing levels.

Immuno-SABER is compatible with widely available sample preparation and microscopy platforms (such as standard wide-field and confocal microscopes or slide scanners), promising easy adoption by research and clinical laboratories. SABER enables higher throughput in two ways. First, it saves sample preparation time by allowing application of multiple primary antibodies in one step, thus alleviating the need for multiple time-consuming cycles of antibody staining. This advantage is particularly important for thicker tissue samples such as whole-mount and ExM preparations (where we imaged six targets in approximately threefold expanded tissues within 3–6 h in contrast to the ~4–5 d that would be required in protocols such as MAP[38]). Second, SABER saves image acquisition time as high signal level supports reduced camera exposures. A 10- to 100-fold improvement in image acquisition can deliver one to two orders of magnitude enhancement of throughput, which is needed for discovery-oriented profiling of cells and tissues and large-scale mapping projects.

To implement Immuno-SABER for new targets, we recommend aiming to conjugate a limited number (1–3 copies) of bridge oligonucleotides per antibody to preserve the antigen recognition efficiency of the antibody and to validate the specificity of the staining by comparison to unconjugated controls. For relative quantifications, a baseline control can be utilized (on the same sample (Supplementary Fig. 4) or on comparable samples (Fig. 3)). As in any signal amplification method, increasing amplification level is expected to yield a wider spread in the population, while moving the mean to higher intensities. For branched amplification, it is

theoretically possible that the small differences in the initial binding might lead to larger variations. However, at the population level, these factors should have an even effect on the sample (unless there is critical internal heterogeneity, like the target being more buried in some locations, which would bias antibody binding for all immunofluorescence studies), as suggested by the consistency of the stainings in Supplementary Fig. 4. Advantageously, Immuno-SABER avoids in situ enzymatic reactions, which are hard to reproduce in a quantitative manner as the enzyme activity is hard to control. For SABER, every step relies on simple DNA–DNA binding that can be primarily modulated by salt and formamide concentration, as well as temperature.

In summary, Immuno-SABER is a simple and effective method for multiplexed and sensitive in situ protein detection with individually programmable signal amplification. Immuno-SABER enables higher throughput for imaging assays ranging from super-resolution studies to centimeter-scale tissue mapping efforts. The SABER strategy is also directly applicable for RNA and DNA targets as we recently demonstrated in our SABER-FISH work[30]. We expect that the unified SABER framework will be useful to a broad range of researchers, complementing single-cell RNA sequencing analysis with the functional information of protein expression, and will prove valuable for a wide spectrum of potential applications including tissue atlases[44,45], tumor and disease profiling, in situ single-cell validation for bulk assays such as flow or mass cytometry, and CITE-Seq[46], as well as digital pathology and biomarker screening and discovery.

Online content

Any methods, additional references, Nature Research reporting summaries, source data, statements of code and data availability and associated accession codes are available at https://doi.org/10.1038/s41587-019-0207-y.

Received: 11 January 2019; Accepted: 27 June 2019;
Published online: 19 August 2019

References

1. Angelo, M. et al. Multiplexed ion beam imaging of human breast tumors. *Nat. Med.* **20**, 436–442 (2014).
2. Levenson, R. M., Borowsky, A. D. & Angelo, M. Immunohistochemistry and mass spectrometry for highly multiplexed cellular molecular imaging. *Lab. Invest.* **95**, 397–405 (2015).
3. Giesen, C. W. et al. Highly multiplexed imaging of tumor tissues with subcellular resolution by mass cytometry. *Nat. Methods* **11**, 417–425 (2014).
4. Wei, L. et al. Super-multiplex vibrational imaging. *Nature* **544**, 465–470 (2017).
5. Gerdes, M. J. et al. Highly multiplexed single-cell analysis of formalin-fixed, paraffin-embedded cancer tissue. *Proc. Natl Acad. Sci. USA* **110**, 11982–11987 (2013).
6. Lin, J. R., Fallahi-Sichani, M. & Sorger, P. K. Highly multiplexed imaging of single cells using a high-throughput cyclic immunofluorescence method. *Nat. Commun.* **6**, 8390 (2015).
7. Lin, J.-R. et al. Highly multiplexed immunofluorescence imaging of human tissues and tumors using t-CyCIF and conventional optical microscopes. *eLife* **7**, e31657 (2018).
8. Gut, G., Herrmann, M. D. & Pelkmans, L. Multiplexed protein maps link subcellular organization to cellular states. *Science* **361**, eaar7042 (2018).
9. Wang, Y. et al. Rapid sequential in situ multiplexing with DNA exchange imaging in neuronal cells and tissues. *Nano Lett.* **17**, 6131–6139 (2017).
10. Schueder, F. et al. Universal super-resolution multiplexing by DNA exchange. *Angew. Chem. Int. Ed. Engl.* **56**, 4052–4055 (2017).
11. Jungmann, R. et al. Multiplexed 3D cellular super-resolution imaging with DNA-PAINT and Exchange-PAINT. *Nat. Methods* **11**, 313–318 (2014).
12. Goltsev, Y. et al. Deep profiling of mouse splenic architecture with CODEX multiplexed imaging. *Cell* **174**, 968–981 (2018).
13. Lundberg, E. et al. Defining the transcriptome and proteome in three functionally different human cell lines. *Mol. Syst. Biol.* **6**, 450 (2010).
14. Bobrow, M., Litt, G. J., Shaughnessy, K. J., Mayer, P. C. & Conlon, J. The use of catalyzed reporter deposition as a means of signal amplification in a variety of formats. *J. Immunol. Methods* **150**, 145–149 (1992).
15. Yarilin, D. et al. Machine-based method for multiplex in situ molecular characterization of tissues by immunofluorescence detection. *Sci. Rep.* **5**, 9534 (2015).
16. Stack, E. C., Foukas, P. G. & Lee, P. P. Multiplexed tissue biomarker imaging. *J. Immunother. Cancer* **4**, 9 (2016).
17. Schweitzer, B. et al. Immunoassays with rolling circle DNA amplification: a versatile platform for ultrasensitive antigen detection. *Proc. Natl Acad. Sci. USA* **97**, 10113–10119 (2000).
18. Nagendran, M., Riordan, D. P., Harbury, P. B. & Desai, T. J. Automated cell-type classification in intact tissues by single-cell molecular profiling. *eLife* **7**, e30510 (2018).
19. Deng, R. et al. DNA-sequence-encoded rolling circle amplicon for single-cell RNA imaging. *Chem* **4**, 1373–1386 (2018).
20. Chen, Y. et al. Mapping 3D genome organization relative to nuclear compartments using TSA-Seq as a cytological ruler. *J. Cell Biol.* **217**, 4025–4048 (2018).
21. Pachl, C. et al. Rapid and precise quantification of HIV-1 RNA in plasma using a branched DNA signal amplification assay. *J. Acquir. Immune Defic. Syndr.* **8**, 446 (1995).
22. Kern, D. et al. An enhanced-sensitivity branched-DNA assay for quantification of human immunodeficiency virus type 1 RNA in plasma. *J. Clin. Microbiol.* **34**, 3196–3202 (1996).
23. Wang, F. et al. RNAscope: a novel in situ RNA analysis platform for formalin-fixed, paraffin-embedded tissues. *J. Mol. Diagn.* **14**, 22–29 (2012).
24. Dirks, R. M. & Pierce, N. A. Triggered amplification by hybridization chain reaction. *Proc. Natl Acad. Sci. USA* **101**, 15275–15278 (2004).
25. Choi, H. M. et al. Programmable in situ amplification for multiplexed imaging of mRNA expression. *Nat. Biotechnol.* **28**, 1208–1212 (2010).
26. Choi, H. M. T. et al. Third-generation in situ hybridization chain reaction: multiplexed, quantitative, sensitive, versatile, robust. *Development* **145**, dev165753 (2018).
27. Wang, Y., Xie, W., Kohman, R. E. & Church, G. M. Multiplexed imaging using same species primary antibodies with signal amplification. Preprint at https://doi.org/10.1101/274456 (2018).
28. Lin, R. et al. A hybridization-chain-reaction-based method for amplifying immunosignals. *Nat. Methods* **15**, 275–278 (2018).
29. Kishi, J. Y., Schaus, T. E., Gopalkrishnan, N., Xuan, F. & Yin, P. Programmable autonomous synthesis of single-stranded DNA. *Nat. Chem.* **10**, 155–164 (2018).
30. Kishi, J. Y. et al. SABER amplifies FISH: enhanced multiplexed imaging of RNA and DNA in cells and tissues. *Nat. Methods* **16**, 533–544 (2019).
31. Chen, F., Tillberg, P. W. & Boyden, E. S. Expansion microscopy. *Science* **347**, 543–548 (2015).
32. Nave, H., Gebert, A. & Pabst, R. Morphology and immunology of the human palatine tonsil. *Anat. Embryol.* **204**, 367–373 (2001).
33. Slijkerman, R. W. et al. The pros and cons of vertebrate animal models for functional and therapeutic research on inherited retinal dystrophies. *Prog. Retin. Eye Res.* **48**, 137–159 (2015).
34. Speel, E. J., Hopman, A. H. & Komminoth, P. Amplification methods to increase the sensitivity of in situ hybridization: play card(s). *J. Histochem. Cytochem.* **47**, 281–288 (1999).
35. Clutter, M. R., Heffner, G. C., Krutzik, P. O., Sachen, K. L. & Nolan, G. P. Tyramide signal amplification for analysis of kinase activity by intracellular flow cytometry. *Cytometry A* **77**, 1020–1031 (2010).
36. Zadeh, J. N. et al. NUPACK: analysis and design of nucleic acid systems. *J. Comput. Chem.* **32**, 170–173 (2011).
37. Uhlen, M. et al. Tissue-based map of the human proteome. *Science* **347**, 1260419 (2015).
38. Ku, T. et al. Multiplexed and scalable super-resolution imaging of three-dimensional protein localization in size-adjustable tissues. *Nat. Biotechnol.* **34**, 973–981 (2016).
39. Chen, F. et al. Nanoscale imaging of RNA with expansion microscopy. *Nat. Methods* **13**, 679–684 (2016).
40. Chang, J. B. et al. Iterative expansion microscopy. *Nat. Methods* **14**, 593–599 (2017).
41. Truckenbrodt, S. et al. X10 expansion microscopy enables 25-nm resolution on conventional microscopes. *EMBO Rep.* **19**, e45836 (2018).
42. Dani, A., Huang, B., Bergan, J., Dulac, C. & Zhuang, X. Superresolution imaging of chemical synapses in the brain. *Neuron* **68**, 843–856 (2010).
43. Moffitt, J. R. et al. High-throughput single-cell gene-expression profiling with multiplexed error-robust fluorescence in situ hybridization. *Proc. Natl Acad. Sci. USA* **113**, 11046–11051 (2016).
44. Regev, A. et al. The Human Cell Atlas. *eLife* **6**, e27041 (2017).
45. Snyder, M. M. et al. Mapping the human body at cellular resolution—the NIH Common Fund Human BioMolecular Atlas program. Preprint at https://arxiv.org/abs/1903.07231 (2019).
46. Stoeckius, M. et al. Simultaneous epitope and transcriptome measurement in single cells. *Nat. Methods* **14**, 865–868 (2017).

47. Takada, S. E. & Engleman, E. G. Evidence for an association between CD8 molecules and the T cell receptor complex on cytotoxic T cells. *J. Immunol.* **139**, 3231–3235 (1987).
48. Beck, M. et al. The quantitative proteome of a human cell line. *Mol. Syst. Biol.* **7**, 549 (2011).
49. Bernstein, H. G. et al. Regional and cellular distribution of neural visinin-like protein immunoreactivities (VILIP-1 and VILIP-3) in human brain. *J. Neurocytol.* **28**, 655–662 (1999).
50. Haverkamp, S. & Wassle, H. Immunocytochemical analysis of the mouse retina. *J. Comp. Neurol.* **424**, 1–23 (2000).

Acknowledgements

We thank C. Cepko, P. Sorger, Z. Maliga and J. Lin for discussion. We thank the Neurobiology Department and the Neurobiology Imaging Facility for instrument support. This facility is supported in part by the Neural Imaging Center as part of NINDS P30 Core Center grant NS072030. We thank M. Manesse, T. Archivald and D. Bowman for help with the FFPE samples, and I. Goldaracena for comments on the manuscript. We thank S. Wang for providing neuronal cultures. This work was supported by grants from the National Institutes of Health (under grants NIH Common Fund 1UG3HL145600/HuBMAP, 1R01EB018659, 1U01MH106011, 1DP1GM133052 and 1R01GM124401), the Office of Naval Research (under grants N00014-16-1-2410, N00014-16-1-2182 and N00014-18-1-2549), the National Science Foundation (under grant CCF-1317291), Harvard Medical School Dean's Initiative and Wyss Institute's Molecular Robotics Initiative to P.Y. G.M.C. was supported by NIH grants (R01NS083898, RM1 HG008525 and R01MH113279), and P.S.K. was supported by an NIH grant (1R01MH113349). J.Y.K. was supported by a National Science Foundation Graduate Research Fellowship. B.J.B. was supported by a Damon Runyon Cancer Research Foundation Fellowship. S.W.L. was supported by HHMI and the National Institutes of Health (grant 5K99EY028215-02). W.X., Y.Z. and S.Y. were partially supported by visiting undergraduate student funding from Fudan University, Tsinghua University and Shanghai Jiaotong University, respectively. S.K.S. was supported by long-term postdoctoral fellowships from EMBO (ALTF 1278- 2015) and the Human Frontier Science Program (HFSP) (LT000048/2016-L).

Author contributions

S.K.S. and Y.W. conceived the study, performed experiments, analyzed the data and wrote the manuscript. J.Y.K. contributed to conceptualization of the study, protocol optimization and experimental design. A.Z., Y.Z., W.X., S.Y. and M.L. provided experimental assistance. K.K., C.Y. and M.C. performed data analysis and visualization. B.J.B. contributed to protocol optimization. S.W.L. provided the retina samples for staining. G.P. contributed to contextualization of SABER application, and provided guidance and tissues for the FFPE study. E.S.B. contributed to the expansion study. P.S.K. contributed to the neuronal study. G.M.C. provided scientific guidance and contributed to study supervision. P.Y. conceived and supervised the study, and wrote the manuscript. All authors edited and approved the manuscript.

Competing interests

S.K.S., Y.W., J.Y.K., B.J.B. and P.Y. are inventors for a US patent application based on this work (PCT/US2018/013019). P.Y. is a co-founder of Ultivue, Inc. and NuProbe Global.

Additional information

Supplementary information is available for this paper at https://doi.org/10.1038/s41587-019-0207-y.

Reprints and permissions information is available at www.nature.com/reprints.

Correspondence and requests for materials should be addressed to S.K.S., Y.W. or P.Y.

Publisher's note: Springer Nature remains neutral with regard to jurisdictional claims in published maps and institutional affiliations.

Methods

Technical details for the experiments are given below. We also provide generalized, step-by-step protocols for antibody–DNA conjugation, purification of conjugated antibodies and performing Immuno-SABER in cells, FFPE samples and fixed cryosections in the Supplementary Protocols.

Additionally, we will keep an updated 'Frequently Asked Questions' section available at http://www.immuno-saber.net/ and http://www.saber-imaging.net/.

Primer exchange reaction sequences and preparation of SABER concatemers. *In vitro extension of primers.* Concatemer extensions were prepared as described previously[30]. Typically, 100-µl reactions were prepared in 1× PBS (diluted from a 10× stock; Thermo Fisher, AM9625) with final concentrations of 10 mM $MgSO_4$, 400–1,000 U ml^{-1} Bst LF polymerase (NEB, M0275L; or McLab, BPL-300), 600 µM each of dATP, dCTP and dTTP (NEB, M0275L), 100 nM of Clean.G (5′-CCCCGAAAGTGGCCTCGGGCCTTTTGGCCCGAGGCCACTTTCG-3′) hairpin[29], 50 nM–1.5 µM hairpin, and water to 90 µl. The Clean.G hairpin has a 5′ stretch of C. Preincubation with Clean.G helps to get rid of the impurities in the dHTP mixtures (made up of dATP, dTTP and dCTP), which may have small amounts of dGTP contamination[29]. After Clean.G incubation for 15 min at 37 °C, 10 µl of 10 µM primer was added to obtain 1 µM final concentration, and the reaction was incubated for another 1–3 h at 37 °C followed by 20 min at 80 °C to heat inactivate the polymerase. Reaction products can be stored at −20 °C for several months. In our demonstrations, PER products were diluted into concatemer hybridization solutions for binding to the bridge sequences. Alternatively, concatemers can be purified and concentrated using a MinElute (Qiagen, 28004) kit with distilled water elution to reduce volume and salt concentration from the reaction condition. Primer sequences and details of the extension conditions utilized for Supplementary Fig. 6 are listed in Supplementary Table 1. These primer sequences were presented as the 3′ tail of the complements of the bridge strands given in Supplementary Table 2 in the following format: 5′-bridge*–TT (spacer nucleotides)–9-nucleotide primer sequence-3′, where the asterisk denotes the reverse complement. For the extensions in Supplementary Fig. 6, the 25-nucleotide tester* bridge was used for all the primers. The strands were obtained from IDT. Primers were synthesized and provided with standard desalting. Hairpins were ordered with 3′ inverted dT modification to ensure they cannot be extended. Owing to the modification, they were ordered with HPLC purification, which is critical for their performance. Details of the primer and hairpin design criteria are described in our previous work[29,30]. For primary concatemers, we utilize concatemers of lengths of up to 600–700 nucleotides on the basis of empirical experience[30].

Gel electrophoresis. After extension, for internal quality control, the lengths of the concatemers were evaluated by diluting 1 µl of in vitro reaction with 19 µl water. For quality control, samples were then run on 1–2% E-Gel EX agarose gels (Thermo Fisher, G402001) for 10 min on the E-gel apparatus (Invitrogen, iBase) alongside a 1 kb Plus DNA Ladder (Invitrogen) and imaged with the SybrGold channel on a Typhoon FLA 9000 scanner.

For the comparison gel in Supplementary Fig. 6, unpurified concatemers were run using 6% Tris–borate–EDTA (TBE)–urea PAGE gels (Thermo Fisher) at 55 °C. The gel was prerun for 1 h before loading the samples. One hundred and sixty nanograms of Quick-Load Purple low-molecular-weight DNA ladder (NEB, N0557S) was loaded as a size reference. The reaction products were diluted 1:7 with 2× urea loading dye and denatured at 95 °C for 5 min. Nine microliters from each sample was loaded on the gel. Both samples and the ladder were denatured. Samples were run for 20 min at 75 V and at 130 V for 1 h. Gels were stained with 1:10,000 SybrGold in 0.5× TBE for 30 min and scanned on a Typhoon FLA 9000 scanner.

Imager strands. SABER imager strands are 20-nucleotide DNA oligomers with fluorophores at the 5′ end. The imagers used for our experiments also carry a 3′ inverted dT modification, which is optional and is not essential for SABER experiments. Imagers were designed to bind the dimers of the primer unit sequence to achieve the stable but easily reversible binding that is necessary for DNA-exchange imaging. Hence the format of the imager sequence is as follows: 5′-fluorophore–TT–primer*–T–primer*–T–inverted dT-3′. They were ordered from IDT with a 5′ fluorophore (Atto488, Atto565, Alexa Fluor 647 or Alexa Fluor 750), 3′ inverted dT modification and HPLC purification. They are named as i.primerID#*. Sequences are listed in Supplementary Table 3.

Branching primers. For stable hybridization of the secondary (branching) concatemers onto the primary concatemers, trimers of the unit repeat sequence were used as bridges, creating a 30-nucleotide hybridization sequence. Hence, branching primers are designed in the format: 5′-p.1*–T–p.1*–T–p.1*–TTT–p.2-3′, where p.1 is the primer used for the primary concatemer and p.2 is the primer for the secondary concatemer.

Similarly, for iterative branching, the tertiary concatemer is designed to use the trimers of primer 2 as the bridge, in the format 5′-p.2*–T–p.2*–T–p.2*–T TT–p.3-3′, where p.3 is the primer for the tertiary concatemer and T's are spacer nucleotides.

Antibody–DNA conjugation and purification. *Conjugation.* The conjugation involves crosslinking of thiol-modified DNA oligonucleotides to lysine residues on antibodies in a non-sequence-specific way. In brief, 25 µl of 1 mM 5′-thiol-modified DNA oligonucleotides (IDT) was activated by 100 mM dithiothreitol (DTT) (Thermo Fisher, 20291) for 2 h at room temperature in the dark, and purified using NAP5 columns (GE Healthcare Life Sciences, 17-0853-02) to remove excess DTT. Antibodies formulated in PBS only (or with sodium azide) were concentrated using 0.5-ml 50-kDa Ambicon Ultra Filters (EMD Millipore, UFC510096) to 2 mg ml^{-1} and reacted with maleimide–PEG_2–succinimidyl ester crosslinkers (Thermo Fisher, 22102) for 1.5 h at 4 °C (100 µg antibodies: 2.5–3.4 µl of 0.85 mg ml^{-1} cross-linker). Antibodies were then purified using 0.5-ml 7-kDa Zeba desalting columns (Thermo Fisher, 89883) to remove excess cross-linkers. Activated DNA oligonucleotides were incubated with antibodies (molar ratio of antibody to single-stranded DNA of ~1:11) overnight at 4 °C. The final conjugated antibodies were washed using 2-ml 50-kDa Amicon Ultra Filters six times to remove non-reacted DNA oligonucleotides. The list of bridge sequences used for conjugation is provided in Supplementary Table 2. The list of antibodies and the corresponding bridge sequences (IDT) used for each staining, as well as the capture and toehold strands for purification is provided in Supplementary Table 4. Conjugated antibodies were diluted at ratios of between 1:50 and 1:200 for immunostaining. A detailed step-by-step protocol for general use is available in the Supplementary Protocols.

Purification. To increase the staining efficiency, conjugated antibodies can optionally be purified using a DNA-toehold-mediated affinity pulldown protocol (Supplementary Fig. 1a). For this, 200 µl of high-capacity streptavidin agarose (Thermo Fisher, 20357) was centrifuged, washed three times using 500 µl of PBS, and incubated with 10 µl of 1 mM biotin-labeled binding sequences in 300 µl PBS with 0.1% Triton X-100 for 30 min at room temperature. The agarose was then washed twice with PBS with 0.1% Triton X-100, followed by blocking with 250 µl of blocking buffer (2% BSA + 0.1% Triton in PBS) for 1 h at room temperature with rotation. The agarose was then centrifuged and resuspended with 200 µl of incubation buffer (1% BSA + 0.1% Triton in PBS) containing the DNA-conjugated antibodies, followed by rotation at 4 °C for 1 h. The sample was centrifuged at 4 °C and washed twice with 200 µl incubation buffer. The bound antibodies were recovered by adding 20 µl of 1 mM toehold strands (listed in Supplementary Table 4) in 200 µl of incubation buffer. After centrifugation, the supernatant was collected and the agarose was washed three times with 300 µl of washing buffer (PBS + 0.1% Triton); supernatant was collected after each wash. The supernatant was pooled together and the buffer was exchanged using 2-ml 50-kDa Amicon Ultra Filters six times to remove toehold DNA oligonucleotides. Binding sequences and toehold sequences were designed using NUPACK (http://www.nupack.org/)[36,51,52] and are provided in Supplementary Table 4.

SDS–PAGE. To examine DNA–antibody conjugation, antibodies were denatured in LDS sample buffer (Thermo Fisher, NP0007) without reducing reagents (for example, DTT or 2-mercaptoethanol) at 90–95 °C for 3 min, and left to cool down to room temperature. The samples were run on 3–8% Tris-acetate PAGE gels (Thermo Fisher, EA03752BOX) in NuPAGE Tris-Acetate SDS Running Buffer (Thermo Fisher, LA0041) at 80 V for 30 min and 120 V for 3.5 h. The gels were stained with SimplyBlue safe stain (Thermo Fisher, LC6060) according to the manufacturer's manual, and imaged using a Biorad Gel Doc EZ imager system. Note that BSA should be avoided in the purification step if the sample needs to be examined using PAGE gels.

Microtubule staining in cell culture and full-width half-maximum analysis. *Cell culture and staining.* BS-C-1 cells (ATCC CCL-26, African green monkey) were grown in DMEM (Gibco, 10564) supplemented with 10% (vol/vol) serum (Gibco, 10437), 50 U ml^{-1} penicillin and 50 µg ml^{-1} streptomycin (Gibco, 15070) and cultured at 37 °C in the presence of 5% CO_2. They were plated on eight-well Ibidi glass-bottom µ-slides (Ibidi, 80826) and grown to 50–60% confluency. For the cell culture experiments in Figs. 2 and 3, cells were fixed with 4% paraformaldehyde (PFA) for 45 min, quenched with 100 mM NH_4Cl in PBS for 20 min and washed with PBS for 5 min. Cells were then permeabilized and blocked in 2% nuclease-free BSA (AmericanBIO, CAS 9048-46-8) with 0.1% Triton in PBS for 30 min. Samples were incubated with DNA-conjugated primary antibodies diluted in incubation buffer (0.1% Triton X-100, 2% nuclease-free BSA, 0.2 mg ml^{-1} sheared salmon sperm DNA, 0.05% dextran sulfate (Millipore, S4030) and 4 mM EDTA (Ambion, AM9260G) in PBS) overnight at 4 °C, and then washed three times with PBS with 0.1% Triton X-100 and 2% BSA for 10 min. Samples were then washed twice with PBS for 5 min and post-fixed using 5 mM $BS(PEG)_5$ (Thermo Fisher, 21581) in PBS for 30 min, followed by quenching in 100 mM NH_4Cl in PBS for 5 min. The incubation with the primary concatemer was performed at 37 °C in 20% formamide (deionized; Ambion, AM9342), 10% dextran sulfate and 0.1% (vol/vol) Tween-20 in 2× saline sodium citrate (SSC) buffer with 0.2 mg ml^{-1} sheared salmon sperm DNA for 3 h. The 650-nucleotide primary concatemers prepared in vitro by PER were diluted in this buffer at a 133 nM final primer concentration (primer concentration in the PER mix is considered a proxy for the concatemer concentration after the reaction, as all primers are expected to be extended by the

catalytic hairpins, which are provided in excess). After concatemer hybridization, the samples were washed for 5 min at room temperature with 45% formamide in PBS and three times for 10 min each with PBS + 0.1% Triton X-100 at 37 °C. Branching hybridization was performed overnight at 37 °C in 30% formamide, 10% dextran sulfate and 0.1% (vol/vol) Tween-20 in 2× SSC with 0.2 mg ml^{-1} sheared salmon sperm DNA and the 450-nucleotide secondary concatemers at a final concentration of 133 nM. Samples were washed for 5 min at room temperature with 45% formamide in PBS and three times for 10 min each with PBS + 0.1% Triton X-100 at 37 °C. Imagers were hybridized at a 1–1.5 µM final concentration in PBS + 0.1% Triton X-100 for 1 h at room temperature (hybridization duration with the imagers can be decreased for faster preparation), followed by a 5-min wash with PBS + 0.1% Triton X-100 and two 5-min washes with PBS. Samples were stained with 4 µg ml^{-1} DAPI (Invitrogen, D1306) in PBS for 10 min and washed twice for 1 min with PBS. Imaging was performed in SlowFade with DAPI (Invitrogen, S36938) embedding medium.

Imaging. For the images shown in Fig. 2a and Supplementary Figs. 2a and 3e, a Leica SP5 confocal microscope with a 63×/1.3 NA glycerol objective was used. A white-light laser (470–670 nm) was used at 650 nm for excitation of Alexa Fluor 647, and a photomultiplier tube (PMT) was used for detection.

Full-width half-maximum analysis. The best focus planes for isolated microtubules were manually selected from *z* stacks. Line plots (2.5 µm) were drawn across isolated microtubules in this single plane image using Fiji[53]. Small rectangular background areas were manually drawn to obtain the background values around selected microtubule lines. Average background was subtracted from the line-plot values. Gaussian curves were fit to the background-subtracted values; FWHM was calculated on the basis of the fits and average values were obtained by analyzing 30–45 line plots from five images per condition using a Python script. A similar calculation was performed for 200-nm dark red FluoSphere beads (Invitrogen, F8807). Distributions arre displayed as box plots. Line plots with multiple discernible peaks were discarded. A two-sample *t* test was performed to check for statistical significance.

Lamin B staining in cell culture for amplification quantification. *Staining.* HeLa cells (human) were cultured and stained following the general protocol as described above for microtubules, with the following changes. Before the secondary antibody incubation, blocking was performed in 2% donkey serum with 1.5 % BSA, 0.1% Triton and 0.2 µg µl^{-1} sheared salmon sperm DNA for 15 min. Secondary antibodies were also diluted in the same buffer, and stained for 1.5 h at room temperature. Post-fixation was done for 10 min with 4% PFA. The following conditions were used for primary concatemer hybridization: 125 nM for 2 h at 37 °C in 20% formamide, 10% dextran sulfate and 0.1% (vol/vol) Tween-20 in 2× SSC with 0.2 mg ml^{-1} sheared salmon sperm DNA. Before and after the concatemer hybridization, a block and wash was done for 10 min with 0.1% Triton X-100 in PBS, 0.2 µg µl^{-1} salmon sperm DNA and 3.3% dextran sulfate for 10 min. Imager hybridization 1 was performed with 1 µM Alexa Fluor 647–i.27* for 75 min at room temperature. For linear amplification samples, imager hybridization 2 was performed similarly with Alexa Fluor 647–i.28*. Branch concatemer hybridization was perfomed for overnight at 37 °C with 100 nM extended concatemer in the same buffer as the primary concatemer hybridization. For branching samples, imager hybridizations 2 and 3 were done with Alexa Fluor 647–i.30* and Alexa Fluor 647–i.25*, respectively. Sequences and extension conditions are listed in Supplementary Table 5.

Imaging. Twenty-one- to 26-plane *z* stacks were imaged using a Zeiss Axio Observer Z1 with a 100×/1.4 NA oil objective. Alexa Fluor 647 (excitation at 590–650 nm, detection at >665 nm) images were acquired with 10% of the LED power at 150-ms exposure, and DAPI (excitation at 300–400 nm, detection at 420–470 nm) with 20% power at 100 ms exposure.

Signal quantification. Maximum projections of the *z* stacks were created using Fiji. DAPI images were acquired and used to create nuclear masks in MATLAB and Image Processing Toolbox. Mean Alexa Fluor 647 signal per pixel was calculated within the mask region for each cell.

SABER application, quantification and analysis on human tonsil formalin-fixed paraffin-embedded sections. *Preparation of formalin-fixed paraffin-embedded tonsil samples and antigen retrieval.* Human specimens were retrieved from the archives of the Pathology Department of Beth Israel Deaconess Medical Center under the discarded and excess tissue protocol as approved in Institutional Review Board (IRB) Protocol 2017P000585. We have complied with all relevant ethical regulations. Five-micrometer sections were cut with a rotary microtome, collected in a water bath at 30 °C, transferred to positively charged glass slides and baked at 60 °C for 2 h. For antigen unmasking, slides were placed on a PT-Link instrument (Agilent), which allows the entire pretreatment process of deparaffinization, rehydration and epitope retrieval (with citrate buffer) to be combined into a single step. Slides were held at 4 °C in PBS until staining. Antigen-retrieved FFPE sections used in the multicolor experiments in Fig. 4 were acquired from Ultivue, Inc.

Staining of antigen-retrieved formalin-fixed paraffin-embedded tonsil samples. After antigen retrieval, sections were optionally stored in PBS at 4 °C for up to 2 weeks. For staining, sections were washed in PBS for 15 min and outlined with a hydrophobic pen (ImmEdge Hydrophobic Barrier PAP Pen; Vector Laboratories, H4000) or enclosed in a removable chamber (Ibidi, 80381). At this stage, mild 1-h prebleaching with 1% H_2O_2 in PBS can optionally be applied (for TSA). This step is not necessary for Immuno-SABER. We incorporated this step for the Ki-67 stainings in Fig. 3 and Supplementary Fig. 5, to keep the conditions similar to TSA preparations, which benefit from a prebleaching step. Samples were blocked for 1 h with PBS containing 2% BSA and 0.1–0.3% Triton X-100, with three buffer exchanges. DNA-conjugated primary antibodies were diluted in the blocking solution supplemented with 0.2 µg ml^{-1} sheared salmon sperm DNA, 0.05% dextran sulfate and optionally 4 mM EDTA, and incubated with the samples overnight at 4 °C in a humidified chamber. The antibodies and respective bridge sequences used for the experiments are listed in Supplementary Table 4. Depending on the antibody, this step can be shortened to 1 h when performed at room temperature. Excess antibodies were removed by washing at room temperature three times for 15 min with PBS containing 2% BSA and 0.1–0.3% Triton X-100, and twice for 5 min with PBS. Bound antibodies were then post-fixed with 5 mM $BS(PEG)_5$ in PBS for 30 min at room temperature, followed by quenching in 100 mM NH_4Cl in PBS for 5 min, and washed for 15 min with PBS with 0.1% Triton X-100 at room temperature. Post-fixation is critical to ensure that the antibodies are not washed away during further labeling and imaging. The incubation with the primary concatemer was performed at 37 °C in 20–30% formamide, 10% dextran sulfate and 0.1% (vol/vol) Tween-20 in 2× SSC with 0.2 mg ml^{-1} sheared salmon sperm DNA for between 1 h and overnight. Concatemers prepared in vitro by PER were diluted in this buffer at a final concentration of 66–150 nM (1:15 to 1:7.5 dilution). For multiplexing, all primary concatemers were incubated simultaneously. After concatemer hybridization, the samples were washed for 5 min at room temperature with 45–50% formamide in PBS and three times for 10 min each with PBS + 0.1% Triton X-100 at 37 °C. For cases where further amplification was desired, branching hybridizations were performed similarly (at 37 °C in 30% formamide, 10% dextran sulfate and 0.1% Tween-20 in 2× SSC with 0.2 mg ml^{-1} sheared salmon sperm DNA for between 1 h and overnight). Bridge and primer sequences for each target and experiment are given in Supplementary Table 4. For the unamplified sample, the unextended primer with a single imager-binding site (equivalent to two repeats of the primer sequence) was incubated at the same concentration instead of the extended concatemer (for CD8a, bc42_2*–TT–p.25-A–p.25-A; for Ki-67, bc42_0*–TT–p.30-A–p.30-A; sequences are given in Supplementary Table 5).

For different tissue types and combinations of targets for multiplexing, experimental conditions may need to be optimized to achieve the best signal level. For primary concatemers, we recommend using sequences of ≤650 nucleotides, for secondary concatemers sequences of ≤450 nucleotides and for tertiary concatemers sequences ≤250 nucleotides on the basis of empirical experience. For iterative amplification, the wash temperatures were raised to 42 °C and the 45–50% formamide in PBS wash step was performed once as a final wash only at the end of all iterations (rather than after each amplification round).

Fluorophore hybridization and dehybridization. Imagers were hybridized at a final concentration of 1–1.5 µM in PBS + 0.1% Triton X-100 for 1–2 h at room temperature, followed by a 5-min wash with PBS + 0.1% Triton X-100 at 37 °C and two 5-min washes with PBS at room temperature. Lengthened hybridization times were used for convenience; for faster protocols, hybridization duration for the imagers can be decreased with similar performance. Samples were stained with 1 µg ml^{-1} DAPI in PBS for 10 min and washed twice for 1 min with PBS. For multiplexing experiments, samples were imaged in PBS shortly after preparation and coverslips were temporarily secured with Fixogum (Marabu). Applying coverslips to the samples for imaging is optional depending on the instrument type. Imagers were removed with a 10-min incubation at room temperature in 50% formamide in PBS, followed by two 5-min washes with PBS at room temperature. A new round of imager hybridization was performed as above.

For experiments with a single round of imager hybridization (no multiplexing or only spectral multiplexing), samples were embedded in SlowFade with DAPI, secured with nail polish and imaged on the same day or embedded with ProLong Diamond (Invitrogen, P36971) and incubated at room temperature overnight for curing (Supplementary Note 2).

Tyramide signal amplification. For FFPE samples, the anti-rabbit IgG Alexa Fluor 647 Tyramide SuperBoost kit (Life Technologies, B40916) was used according to the manufacturer's recommendations. The optional step of 1-h prebleaching with 1% H_2O_2 in PBS was applied. Tyramide–Alexa Fluor 647 was incubated for 2.5 min, 7.5 min and 10 min. Longer incubation times (≥7.5 min) were observed to cause increased blurring of the signal, making shorter incubation times more favorable (as suggested by the manufacturer).

Fluorescence imaging. FFPE samples in Figs. 2 and 3, and Supplementary Figs. 2, 3, 4, 5b,c and 7a were imaged with an Olympus VS-120 system equipped with an Orca R2 monochrome (16 bit) camera using a 20×/0.75 NA air objective with a pixel size of 0.320 µm, and single-plane tile scans were acquired. For Fig. 3 staining,

exposure times of 35 ms and 30 ms were used for DAPI and Ki-67, respectively. For the CD8a staining in Figs. 1 and 2, an exposure time of 350 ms was used.

For the expanded views in Fig. 3f and Supplementary Fig. 5f a Leica SP5 confocal microscope with 63×/1.3 NA glycerol objective was used. A white light laser (470–670 nm) was used at 650 nm for excitation of Alexa Fluor 647, and a PMT was used for detection.

Multiplex FFPE samples in Fig. 4 and Supplementary Fig. 7b were imaged with a Perkin Elmer Vectra Polaris microscope in whole-slide scanning configuration with a 20×/0.80 NA air objective. For Fig. 4c, imagers were first hybridized for three of the targets (as depicted in the figure), followed by nuclear DAPI staining, washing, coverslipping and whole-section imaging in five channels (three markers plus DAPI and autofluorescence). This was followed by dehybridization as described above. The second set of imagers was similarly hybridized and the sample was reimaged. Images obtained in .qptiff format were converted to .tif with Imaris software and aligned using the 'Align by line ROI' plugin on Fiji using the DAPI fluorescence in each cycle; overlays for display were assembled in Adobe Photoshop.

Signal quantification. For quantification of signal amplification in CD8a labeling of tonsil samples in Fig. 2 and Supplementary Fig. 3b,d, ROIs covering 0.03–1.2 mm^2 tile scan areas were selected after manual inspection to exclude areas with autofocusing errors or sectioning imperfections, and a CellProfiler routine was used first to remove masked autofluroescent structures identified in an independent channel (using global robust thresholding) and then to calculate mean fluorescence signal per pixel for cell regions masked via thresholding of the CD8a signal[54]. For masking of the labeled structures, edges were enhanced by the Canny edge-finding method with automatic threshold calculation. Then, global robust background thresholding was applied. The upper outlier fraction and correction factor for thresholding were adjusted manually to compensate for the difference in overall signal level under different amplification conditions. The background was calculated by averaging the CD8a fluorescence signal of the tissue regions (ensured by the presence of DAPI) outside of the masked signal regions (after dilation of the masked pixels). The final intensity value was obtained by subtracting the mean background value for each ROI from the average signal value for masked cells. Fold amplification of signal was calculated by dividing the mean background-subtracted fluorescence by the unamplified sample (for linear SABER; Fig. 2c,e) or by the linear amplification sample (for branched SABER; Supplementary Fig. 3b,d). Figures were prepared for display using OMERO for ROI selection and scaling[55].

Nuclear segmentation, analysis of single-nuclei intensity distribution and quantification of fold amplification of signal. We annotated the contours of all the nuclei for 80 patches of 128 × 128 pixels. This dataset was then augmented eightfold using reflections and rotations, resulting in a dataset of 640 images. For each image, an equal number of non-contour pixels were randomly selected to represent the complementary class in the machine learning algorithm. We trained a variant of the U-Net model[56], adding batch normalization[57] and residual learning[58], to classify pixels in two classes (class 1, nuclei contours; class 2, background and nuclei interiors). We used our own implementation in TensorFlow (hyperparameters are given in Supplementary Note 3). The approximate center of each nucleus was then identified through the regional maxima of a Gaussian-blurred version of the inverted contour probability class. These regional maxima were used as seed points for applying a marker-controlled watershed transform. Background objects were eliminated on the basis of mean intensity and area. For estimation of the fold amplification of signal, mean signal intensity from all the nuclei in each tissue sample was summed to obtain the total Ki-67 signal level. Then, the total signal for each sample was divided by the total signal for the unamplified condition. Total values were not corrected for variation in the number of cells in each section (tissue samples are consecutive sections from the same tissue). Histograms that show the distribution of Ki-67 signal across individual cells were plotted using Python.

SABER application and quantification on mouse retina cryosections. *Sample preparation.* All animal procedures complied with all relevant ethical regulations and were in accordance with the National Institute for Laboratory Animal Research Guide for the Care and Use of Laboratory Animals as approved by the Harvard Medical School Committee on Animal Care. Animals were given a lethal dose of sodium pentobarbital (120 mg kg^{-1}) (MWI, 710101) and enucleated immediately. Eyes were removed and fixed in PFA for 15–30 min. Following dissection, retinas were immersed in 30% sucrose overnight before freezing in TFM (EMS, 72592) and cryosectioning at ~30–40 µm. Eight-well Ibidi glass-bottom µ-slides were treated with 0.3 mg ml^{-1} poly-D-lysine for at least 30 min, followed by three washes in PBS. Retina sections were immobilized onto the glass and stored at −20 °C. Sections were washed three times with Tris-buffered saline (TBS) + 0.3% Triton X-100 for 10 min. Samples were then permeabilized and blocked in 5% normal donkey serum (Jackson ImmunoResearch, 017-000-001) with 0.2 mg ml^{-1} sheared salmon sperm DNA and 0.1–0.3% Triton X-100 in PBS for 2 h. Samples were incubated with DNA-conjugated primary antibodies diluted in the incubation buffer (0.1% Triton X-100, 5% normal donkey serum, 0.2 mg ml^{-1} sheared salmon sperm DNA, 0.05% dextran sulfate and 5 mM EDTA in PBS) overnight at 4 °C, and then washed three times with PBS with 0.1% Triton X-100, 1% normal donkey serum and 5 mM EDTA for 30 min. Samples were then washed twice with PBS for 5 min and post-fixed using 5 mM $BS(PEG)_5$ in PBS for 30 min, followed by washing in PBS for 2 min and quenching in 100 mM NH_4Cl in PBS or 1× TBS for 10 min.

Immuno-SABER. Extended concatemers were diluted in the 1:7.5 to 1:20 range (depending on the target density) in incubation buffers for overnight hybridization at room temperature. The following two concatemer hybridization buffers were used: buffer 1 (40% formamide, 10% dextran sulfate, 0.1% Triton X-100, 0.02% sodium azide and 5 mM EDTA in PBS) and buffer 2 (30% formamide, 10% dextran sulfate, 0.1% Triton X-100, 0.02% sodium azide and 5 mM EDTA in PBS). Buffer 1 was used for incubation with primary concatemers and buffer 2 was used for branching concatemers. Excess concatemers were removed by washing with 45% formamide, 0.1 % Triton X-100 and 5 mM EDTA in PBS for 30 min and twice with 30% formamide, 0.1 % Triton X-100 and 5 mM EDTA in PBS for 30 min at room temperature. For branched conditions, 45% formamide was replaced with 40% formamide for the first wash. For the multiplexed imaging experiment, all primary concatemers were incubated simultaneously. Bridge and primer sequences for each target and experiment are given in Supplementary Table 4.

To quantify linear SABER amplification for cone arrestin, the amplification samples were incubated with SABER concatemers extended from tester*–TT–p.28. The unamplified samples were hybridized with the unextended primer tester*–TT–p.28-a–p.28, which carries one imager-binding site (equivalent to two repeats of the primer sequence) instead of the extended concatemer (at the same final concentration). For quantification of branched SABER for cone arrestin, the branching sample was first incubated with the primary concatemers extended from tester*–TT–p.28, followed by incubation with secondary concatemers extended from the 28*–T–28*–T–28*–TTT–p.25 primer.

For iterative SABER quantification for SV2, the unamplified sample was hybridized with the unextended primer bc42_3*–TT–p.27-a–p.27. The linear amplification sample was hybridized with the primary concatemer extended from bc42_3*–TT–p.27. The branching sample additionally hybridized with the secondary concatemer 27*–T–27*–T–27*–TTT–p.28. The iterative amplification sample was additionally hybridized to the tertiary concatemer extended from 28*–T–28*–T–28*–TTT–p.32. Sequences are listed in Supplementary Table 5.

Fluorescence imaging. Fluorophore-labeled imager strands were diluted to 250 nM–1 µM final concentration range in 0.1% Triton X-100 in PBS, and were incubated with samples for 30 min, followed by washing using 0.1% Triton X-100 in 0.5× PBS three times. Samples were left in PBS during image acquisition. For multiplexing, imager strands were dehybridized by incubating three times with 0.1× PBS and 30% formamide for 10 min, followed by three 5-min washes with 1× PBS to remove the residual formamide before rehybridization of imager strands as above.

For ten-color multiplexing, the entire experiment was done using seven exchange rounds (round 1, calbindin and vimentin; round 2, GFAP and PKCα; round 3, collagen IV and calretinin; round 4: rhodopsin; round 5, VLP1; round 6, SV2; round 7: cone arrestin) with an average of 1.5 h per round (including 30 min for imager hybridization, 15 min for washing of excess imager strands, 15 min for imaging and 30 min for imager strand displacement). It should be noted that the duration for each step is sample dependent, with thicker samples requiring a longer time to ensure complete penetration and signal removal. To ensure the best signal and simplify the multiplexed experimental design, we allowed excess time for each step; however, it is possible to shorten incubation and washing times upon optimization.

All images for mouse retina sections were acquired using a Zeiss Axio Observer with LSM 710 scanning confocal system with a 20×/0.8 NA air objective. The images were 512 × 512 pixels or 1,024 × 1,024 pixels and acquired at acquisition speed 7. Each image was acquired with frame averaging of two. Atto488 was visualized using a 488-nm laser; Atto565 was visualized using a 546-nm laser; and Alexa Fluor 647 was visualized using a 633-nm laser. To remove imager strands, samples were washed three times with 30% formamide and 0.1% Triton X-100 in 0.1× PBS. The samples were left in PBS during imaging. Acquired images were scaled and colored for display using Fiji[53] and Photoshop.

Tyramide signal amplification. For retina cryosections, Alexa Fluor 647 TSA kit 6 with HRP–goat anti-mouse IgG (Life Technologies, T20916) was used following the manufacturer's recommendations, without the optional prebleaching step and with a 7.5-min tyramide incubation.

Quantification. For quantification of signal amplification in retina samples (SV2 and cone arrestin), the mask regions were selected manually using Fiji, and mean fluorescence intensity was calculated. The background was calculated by averaging the fluorescence signal of six randomly selected regions outside the retinas. The final fold-amplification values were obtained by subtracting the background value from the average signal value for each condition and normalizing that by the unamplified condition (Fig. 2d and Supplementary Fig. 5d) or the linear condition (Supplementary Fig. 3c,d).

SABER application on whole-mount retina samples. *Sample preparation and staining.* Whole-mount retina staining was performed on the free-floating samples, which allowed reagents to penetrate from both sides of retinas. The sample preparation was conducted with a similar protocol as above but with longer incubation and wash times. DNA-conjugated primary antibodies were incubated for 40 h at 4 °C, and washed three times for 1 h. DNA extensions were incubated for 40 h at room temperature, and washed three times for 1 h. Bridge and primer sequences for each target are given in Supplementary Table 4. Fluorescent oligonucleotides were incubated for 2 h at room temperature, followed by three 30 min washes with 0.5× PBS. For imaging, retinas were flattened by creating four incisions and mounted on a glass slide. After flattening, the thickness of whole-mount retina samples was typically ~160 to 180 µm.

Imaging. The images were acquired using a Zeiss Axio Observer with an LSM 710 scanning confocal system with a 10×/0.45 NA air objective. A *z* stack of 98 sections with 1-µm spacing was taken for each target.

PER sequence crosstalk analysis. For microtubule staining in Supplementary Fig. 6, BS-C-1 cells were grown in glass-bottomed 96-well plate (Ibidi, 89626) with 5,000 cells per well. Cells were fixed with 4% PFA for 15 min, and quenched with 50 mM NH_4Cl in PBS for 7 min. Cells were then permeabilized and blocked in 0.1% Triton X-100, 0.1% Tween-20, 2% nuclease-free BSA (AmericanBIO, CAS 9048-46-8) and 0.2 mg ml^{-1} sheared salmon sperm DNA (Thermo Fisher, AM9680) in PBS for 1 h. Samples were incubated with DNA-conjugated primary antibodies diluted in incubation buffer (0.05% Triton X-100, 0.05% Tween-20, 2% nuclease-free BSA, 0.2 mg ml^{-1} sheared salmon sperm DNA, 0.05% dextran sulfate (Millipore, S4030) and 5 mM EDTA in PBS) overnight at 4 °C, and then washed with washing buffer (0.05% Triton X-100, 0.05% Tween-20, 2% nuclease-free BSA and 5 mM EDTA in PBS) five times (1–2 min for the first two washes and 10 min for the other three washes). Samples were washed with PBS twice and post-fixed using 5 mM $BS(PEG)_5$ in PBS for 1 h, followed by quenching in TBS for 10 min. Concatemer and imager hybridizations were performed as described for the retina cryosections.

For cognate wells, 20 nM of the corresponding imager strands were incubated, while for crosstalk wells, all other imager strands were incubated with 20 nM for each imager strand. The samples were imaged using a Zeiss Axio Observer Z1 with a 20×/0.8 NA air objective. For signal quantification, the bright-field images were acquired and used to create masks in MATLAB. Average fluorescence signals were calculated within the mask region. The background was calculated as the average fluorescence signals outside the cells. The final fluorescence intensity was the average fluorescence intensity within cell masks minus the background intensity.

Expansion microscopy. The PER primer sequences were modified with acrydite at the 5′ end (IDT), and extended as above. Mouse retina samples were stained with DNA-conjugated antibodies, followed by concatemer hybridization as above for retina cryosections. After washing away excess concatemers, a layer of expandable gel was formed according to the original expansion microscopy protocol[31]. In brief, samples were incubated in monomer solution (1× PBS, 2 M NaCl, 8.625% (wt/vol) sodium acrylate, 2.5% (wt/vol) acrylamide and 0.15% (wt/vol) *N*,*N*′-methylenebisacrylamide) with ammonium persulfate (APS) and teramethylethylenediamine (TEMED) on ice in open air for 20 min. A gelation chamber was then constructed by placing a #1 coverglass on each side of the tissue section. The specimens were transferred to a humidified incubator and left at 37 °C for 2 h. The samples were then digested using proteinase K (New England BioLabs, P8107S) at a 1:100 dilution in digestion buffer (50 mM Tris pH 8, 1 mM EDTA, 0.5% Triton X-100 and 0.8 M guanidine HCl) at 37 °C overnight. The digested samples were then expanded in excess volumes of deionized water. To prevent expanded samples from shrinkage, they were re-embedded in a non-expandable gel (3% acrylamide, 0.15% *N*,*N*′-methylenebisacrylamide with 0.05% APS, 0.05% TEMED). The gel was placed on a bind-silane-treated #1.5 coverglass and immersed in the gel solution on ice for 20 min, followed by gelation at 37 °C for 1.5 h. Five microliters of bind-silane reagent (GE, GE17-1330-01) was diluted with 8 ml of ethanol, 1.8 ml of deionized water and 200 µl of acetic acid. For coating, coverslips were washed with deionized water followed by 100% ethanol and then incubated with bind-silane and air-dried. After re-embedding, imager strands were applied as for normal cryosections, but with longer washing (6 × 10 min), and were imaged as above in regular retina tissue section imaging. Dehybridization times were also extended to six 10-min incubations.

For the primary neuron culture, the culture was grown on a 12-mm-diameter round #1 coverslips, and stained with anti-Bassoon and anti-Homer1b/c antibodies, followed by DNA-conjugated anti-mouse and anti-rabbit secondary antibodies. The primary antibodies were stained in 5% normal donkey serum with 0.1% Triton X-100, and the secondary antibodies were stained in 5% normal donkey serum with 0.1% Triton X-100, 5 mM EDTA and 0.2 mg ml^{-1} sheared salmon sperm DNA. Concatemer incubations were done as for retina cryosections. The expandable gel (19% (wt/vol) sodium acrylate, 10% (wt/vol) acrylamide, 0.05% (wt/vol) *N*,*N*′-methylenebisacrylamide in PBS) was formed by placing the coverslip against a parafilm sheet with 20 µl of expansion gel solution in between. The gel was then digested and expanded as above. The gel was transferred to a coverslip dish (Ibidi, 81148) and was incubated with the imager strands (Atto488–i.30* and Atto565–i.26*) in 0.5× PBS without re-embedding and left in 0.5× PBS during confocal imaging, which gave a similar expansion factor of approximately threefold. The imager strands were incubated for 30 min followed by three 10-min washes using 0.5× PBS. After imaging, the imager strands were washed five times for 10 min, and imaging was performed as described above for retina cryosections.

For TCEP reduction of fluorophores in expanded samples, the samples were incubated with 50 mM TCEP (Sigma, 646547) diluted in 1× PBS and the fluorescence signal was monitored in a time course of 10 min.

Statistics and reproducibility. Cell experiments in Fig. 2b and Supplementary Figs. 2a–c, 3e,f and 4 were performed a number of times with similar results before the final data were quantified for a single experiment. All retina histology experiments (Figs. 2d–f, 5 and 6, and Supplementary Figs. 2d, 3c,d, 5d and 9) were conducted at least twice with similar results, except the controls in Supplementary Fig. 8, which were performed as a single dataset with internal controls. The FFPE stainings in Figs. 2 and 3, and Supplementary Figs. 3b–d, 5 and 7a were separately tested in at least two independent optimization experiments, before the quantification on one dataset from consecutive sections from the same source sample. For FFPE sections, single-, double- and triple-antibody stainings were performed separately on multiple occasions before the four-color and six-color multiplexed experiments in Fig. 4 and Supplementary Fig. 7b were performed on the same experiment day with consecutive sections from the same source tissue. The in vitro reactions in Supplementary Fig. 6a were individually optimized and each was tested multiple times before the combined gel run. Cell experiments in Supplementary Fig. 6 were repeated twice with similar results. The plots in Supplementary Figs. 1c, 2b, 8b and 9d are specific to the image shown, and are representative of the overall tendency of the measurements in the respective dataset. Further internal controls through the optimization phase, including negative controls with omission of the antibodies or other components, and signal patterns matching expected morphologies, further increase our confidence in the consistency and reproducibility of the technique in multiple contexts.

Reporting Summary. Further information on research design is available in the Nature Research Reporting Summary linked to this article.

Data availability

The data that support the findings of this study will be provided by the corresponding authors upon reasonable request.

Code availability

The deep learning algorithm and test dataset for automated identification of nuclear contours in tonsil tissues are available at https://github.com/HMS-IDAC/UNet. The MATLAB code for nuclear segmentation is available at https://github.com/HMS-IDAC/SABERProbMapSegmentation.

References

51. Pierce, N. A. & Dirks, R. M. A partition function algorithm for nucleic acid secondary structure including pseudoknots. *J. Comput. Chem.* **24**, 1664–1677 2003).
52. Dirks, R. M. & Pierce, N. A. An algorithm for computing nucleic acid base-pairing probabilities including pseudoknots. *J. Comput. Chem.* **25**, 1295–1304 (2004).
53. Schindelin, J. et al. Fiji: an open-source platform for biological-image analysis. *Nat. Methods* **9**, 676–682 (2012).
54. Carpenter, A. E. et al. CellProfiler: image analysis software for identifying and quantifying cell phenotypes. *Genome Biol.* **7**, R100 (2006).
55. Allan, C. et al. OMERO: flexible, model-driven data management for experimental biology. *Nat. Methods* **9**, 245–253 (2012).
56. Ronneberger, O., Fischer, P. & Brox, T. U-Net: convolutional networks for biomedical image segmentation. Preprint at https://arxiv.org/abs/1505.04597 (2015).
57. Ioffe, S. & Szegedy, C. Batch normalization: accelerating deep network training by reducing internal covariate shift. Preprint at https://arxiv.org/abs/1502.03167 (2015).
58. He, K., Zhang, X., Ren, S. & Sun, J. Deep residual learning for image recognition. Preprint at https://arxiv.org/abs/1512.03385 (2015).

nature research

Corresponding author(s): Sinem K. Saka, Yu Wang, Peng Yin

Last updated by author(s): June 05, 2019

Reporting Summary

Nature Research wishes to improve the reproducibility of the work that we publish. This form provides structure for consistency and transparency in reporting. For further information on Nature Research policies, see Authors & Referees and the Editorial Policy Checklist.

Statistics

For all statistical analyses, confirm that the following items are present in the figure legend, table legend, main text, or Methods section.

n/a	Confirmed	
☐	☒	The exact sample size (*n*) for each experimental group/condition, given as a discrete number and unit of measurement
☐	☒	A statement on whether measurements were taken from distinct samples or whether the same sample was measured repeatedly
☒	☐	The statistical test(s) used AND whether they are one- or two-sided *Only common tests should be described solely by name; describe more complex techniques in the Methods section.*
☒	☐	A description of all covariates tested
☒	☐	A description of any assumptions or corrections, such as tests of normality and adjustment for multiple comparisons
☒	☐	A full description of the statistical parameters including central tendency (e.g. means) or other basic estimates (e.g. regression coefficient) AND variation (e.g. standard deviation) or associated estimates of uncertainty (e.g. confidence intervals)
☐	☒	For null hypothesis testing, the test statistic (e.g. *F*, *t*, *r*) with confidence intervals, effect sizes, degrees of freedom and *P* value noted *Give P values as exact values whenever suitable.*
☒	☐	For Bayesian analysis, information on the choice of priors and Markov chain Monte Carlo settings
☒	☐	For hierarchical and complex designs, identification of the appropriate level for tests and full reporting of outcomes
☐	☒	Estimates of effect sizes (e.g. Cohen's *d*, Pearson's *r*), indicating how they were calculated

Our web collection on statistics for biologists contains articles on many of the points above.

Software and code

Policy information about availability of computer code

Data collection	Commercial softwares licensed by microscopy companies were utilized: Zeiss Zen 2012 (for LSM 710), Leica LAS AF (for Leica SP5), Zeiss Zen 2.3 Pro Blue edition (for LZeiss Axio Observer Z1), Olympus VS-ASW (for Olympus VS120), PerkinElmer Phenochart (version 1.0.2) .
Data analysis	Open-source Python (3.6.5), TensorFlow (1.12.0), and Deep Learning packages have been utilized for machine learning-based nuclei identification (the algorithm and code is available at https://github.com/HMS-IDAC/UNet). We used Matlab (2017b) for watershed-based nuclear segmentation using the identified nuclear contours. Python 3.6 was used for the FWHM calculations, as well as plotting of histograms. We used MATLAB and the Image Processing Toolbox R2016a (The MathWorks, Inc., Natick, Massachusetts, United States) for quantifications in mouse retina sections and for Supplementary Fig. 4. We utilized Cell Profiler 3.1.5 for the quantifications of signal amplification in FFPE samples in Figure 2 and 3. FIJI (version 2.0.0-rc-69/1.52n) was utilized for ROI selections and format conversions. HMS OMERO (version 5.4.6.21) was used for viewing images and assembling figure panels.

For manuscripts utilizing custom algorithms or software that are central to the research but not yet described in published literature, software must be made available to editors/reviewers. We strongly encourage code deposition in a community repository (e.g. GitHub). See the Nature Research guidelines for submitting code & software for further information.

Data

Policy information about availability of data

All manuscripts must include a data availability statement. This statement should provide the following information, where applicable:

- Accession codes, unique identifiers, or web links for publicly available datasets
- A list of figures that have associated raw data
- A description of any restrictions on data availability

Data and Software Availability: The data and essential custom scripts for image processing will be made available from the corresponding authors P.Y. (py@hms.harvard.edu), S.K.S. (Sinem.Saka@wyss.harvard.edu), and Y.W. (yuwang01@fas.harvard.edu) upon request. The deep learning algorithm and test dataset for automated identification of nuclear contours in tonsil tissues is available on https://github.com/HMS-IDAC/UNet . The MATLAB code for nuclear segmentation is

available on: https://github.com/HMS-IDAC/SABERProbMapSegmentation .

Field-specific reporting

Please select the one below that is the best fit for your research. If you are not sure, read the appropriate sections before making your selection.

☒ Life sciences ☐ Behavioural & social sciences ☐ Ecological, evolutionary & environmental sciences

For a reference copy of the document with all sections, see nature.com/documents/nr-reporting-summary-flat.pdf

Life sciences study design

All studies must disclose on these points even when the disclosure is negative.

Sample size	Each FFPE experiment batch were performed on consecutive sections from the same source, each containing over 600,000 cells. Due to large number of single cells with tens of distinct germinal center morphologies being present in each section, ROIs from different parts of a whole section was used for quantification of signal improvement for each condition (consecutive sections were used for all the conditions of one quantification experiment). Number of ROIs are noted in the respective figure legends. For quantifications in retina samples, due to conserved staining morphology and low sample-to-sample variability n = 6 z-stacks were acquired from at least 2 retina sections. For Supplementary Fig. 4, minimum 5 z-stacks were acquired for each condition to collect images of 18-45 cells. Number of cells are reported in the graphs.
Data exclusions	Parts of the FFPE tissue sections were excluded from analysis due to automated imaging related aberrations (out-of-focus areas) or tissue preparation aberrations (folding of the thin sections at the edges, or uneven thickness at the edge areas). For FWHM calculations in Supplementary Fig. 2, ROIs that yield lineplots with more than one automatically detected peak were discarded to avoid deviations due to multiple peaks. For Supplementary Fig. 4 cells in the samples were excluded when an external bright fluorescent particle (dust speck, dye aggregate etc.) coincided with the nuclei (as confirmed by manual inspection of the images). The exclusion criteria were pre-established.
Replication	Each FFPE experiment batch were performed on consecutive sections from the same source, each containing over 600,000 cells. For evaluation and quantification of our method, multiple biological replicates were not accumulated in order to avoid the error that would be introduced by the natural biological and preparation variation, and to avoid unnecessary use of human tissue material. In the case of the mouse retina quantifications a minimum of two distinct retinal sections were imaged, and each experiment was performed at least twice. For Supplementary Fig. 4 dataset, 16 different conditions were prepared and each were imaged multiple times (before linear, after linear, before branch, after branch). Although the data was not pooled together for the statistics reported in the figure, low cell-to-cell variability was observed and high consistency was seen across the samples for comparable conditions, suggesting low sample to sample variability.
Randomization	Randomization was not necessary for this study.
Blinding	Blinding was not possible as experimental conditions were mostly evident from the image data.

Reporting for specific materials, systems and methods

We require information from authors about some types of materials, experimental systems and methods used in many studies. Here, indicate whether each material, system or method listed is relevant to your study. If you are not sure if a list item applies to your research, read the appropriate section before selecting a response.

Materials & experimental systems

n/a	Involved in the study
☐	☒ Antibodies
☐	☒ Eukaryotic cell lines
☒	☐ Palaeontology
☐	☒ Animals and other organisms
☐	☒ Human research participants
☒	☐ Clinical data

Methods

n/a	Involved in the study
☒	☐ ChIP-seq
☒	☐ Flow cytometry
☒	☐ MRI-based neuroimaging

Antibodies

Antibodies used	The full list is also available in Supplementary Information, Supplementary Table 4. Ki-67 Cell Signaling #9129, clone: D3B5 (formulated in PBS, Lot: 2), diluted 1:100-1:250 after conjugation CD8a Cell Signaling #85336 clone: D8A8Y (formulated in PBS, Lot: 4) diluted 1:150 after conjugation PD-1 Cell Signaling #43248, clone: EH33 (formulated in PBS, Lot: 2), diluted 1:150 after conjugation IgA Jackson ImmunoResearch #109-005-011 (Lot: 134868), diluted 1:150 after conjugation

CD3e Cell Signaling #85061 clone: D7A6E(TM) XP(R) (formulated in PBS, Lot:2), diluted 1:150 after conjugation

IgM Jackson ImmunoResearch #709-006-073 (Lot: 133627), diluted 1:150 after conjugation

Lamin B Santa Cruz sc-6216 clone:C-20, (Lot: E1115), diluted 1:100

Alpha-Tubulin ThermoFisher #MA1-80017 (multiple lots), diluted 1:50 after conjugation

Cone arrestin Millipore #AB15282 (Lot: 2712407), diluted 1:100 after conjugation

GFAP ThermoFisher #13-0300 (Lot: rh241999), diluted 1:50 after conjugation

SV2 HybridomaBank, Antibody Registry ID: AB_2315387, in house production, diluted 1:25 after conjugation

PKCα Novus #NB600-201, diluted 1:50 after conjugation

Collagen IV Novus #NB120-6586, diluted 1:50 after conjugation

Rhodopsin EnCor Bio #MCA-A531, diluted 1:50 after conjugation

Calbindin EnCor Bio #MCA-5A9, diluted 1:25 after conjugation

Vimentin Cell Signaling #5741S, diluted 1:50 after conjugation

Calretinin EnCor Bio #MCA3G9, diluted 1:50 after conjugation

VLP1 EnCor Bio #MCA-2D11, diluted 1:25 after conjugation

Bassoon Enzo ADI-VAM-#PS003, diluted 1:500

Homer1b/c ThermoFisher #PA5-21487, diluted 1:250
Supplementary
Anti-rabbit IgG (to detect Ki-67 and Homer1b/c indirectly) Jackson ImmunoResearch # 711-005-152 (Multiple lots), 1:90 after conjugation

Anti-mouse IgG (to detect Bassoon indirectly) Jackson ImmunoResearch #715-005-151) (Multiple lots), diluted 1:100 after conjugation

Anti-goat IgG (to detect Lamin B indirectly) Jackson ImmunoResearch # 705-005-147) (Lot: 125860), diluted 1:75 after conjugation

Alternative antibodies used to validate colocalization of VLP1 and Calretinin in Supplementary Fig. 8d-f:
Calretinin (SantaCruz #SC-365956; EnCor Bio #CPCA-Calret; EnCor Bio #MCA-3G9 AP), VLP1 (EnCor Bio #RPCA-VLP1; EnCor Bio #CPCA-VLP1; EnCor Bio #MCA-2D11). All diluted 1:100.

Fluorophore-conjugated secondary antibodies used for reference imaging:
anti-rat-Alexa647 (ThermoFisher #A-21472, 1:200), anti-rabbit-Alexa488 (ThermoFisher #A-21206, 1:200), anti-rabbit-Atto488 (Rockland #611-152-122S, Lot:33901, 1:500), anti-mouse-Alexa647 (ThermoFisher #A-31571, 1:400), anti-goat-Alexa647 (ThermoFisher # A-21447, 1:200), anti-rabbit-Alexa647 (Jackson ImmunoResearch, 711-605-152, Lot: 125197, 1:300).

Validation

All antibodies used are from commercial sources as described. Only antibodies that have been validated by the vendor with in vitro and in situ experiments (for IHC and IF, with images available on the websites) and/or heavily used by the community with publication in several references were used. The validation and references for each are publicly available on the respective vendor websites that can reached via the catalog numbers listed above. In our experiments, IF patterns matched the distribution of cell types these antibodies were expected to label based on the literature both before and after conjugation with DNA strands.

Eukaryotic cell lines

Policy information about cell lines

Cell line source(s)	BS-C-1 cells and HeLa cells
Authentication	Cell lines were not authenticated (not relevant for the experiment or results)
Mycoplasma contamination	Cell lines were not tested for mycoplasma contamination (not relevant for the experiment or results)
Commonly misidentified lines (See ICLAC register)	No commonly misidentified cell lines were used.

Animals and other organisms

Policy information about studies involving animals; ARRIVE guidelines recommended for reporting animal research

Laboratory animals	Wild-type CD1 mice (male and female) age P13 or P17 were used for retina harvest.
Wild animals	The study did not involve wild animals.
Field-collected samples	The study did not involve samples collected from the field.
Ethics oversight	All animal procedures were in accordance with the National Institute for Laboratory Animal Research Guide for the Care and Use of Laboratory Animals and approved by the Harvard Medical School Committee on Animal Care.

Note that full information on the approval of the study protocol must also be provided in the manuscript.

Human research participants

Policy information about studies involving human research participants

Population characteristics	We have only used exempt tissue sections for technical demonstration, since we do not derive any biological conclusions, the population characteristics is not relevant for this methodological study.
Recruitment	Not relevant for this study.
Ethics oversight	Human specimens were retrieved from the archives of the Pathology Department of Beth Israel Deaconess Medical Center under the discarded/excess tissue protocol as approved in Institutional Review Board (IRB) Protocol #2017P000585. Informed inform consent was waived on the basis of minimal risk to participants (which is indirect and not based on prospective participation by patients).

Note that full information on the approval of the study protocol must also be provided in the manuscript.

nature biotechnology

SUPPLEMENTARY INFORMATION

https://doi.org/10.1038/s41587-019-0207-y

In the format provided by the authors and unedited.

Immuno-SABER enables highly multiplexed and amplified protein imaging in tissues

Sinem K. Saka[1,2,11]*, Yu Wang[1,2,3,11]*, Jocelyn Y. Kishi[1,2], Allen Zhu[1,2], Yitian Zeng[1,3], Wenxin Xie[1,3], Koray Kirli[4], Clarence Yapp[5,6], Marcelo Cicconet[5], Brian J. Beliveau[1,2,10], Sylvain W. Lapan[3], Siyuan Yin[1,3], Millicent Lin[1,3], Edward S. Boyden[7], Pascal S. Kaeser[8], German Pihan[9], George M. Church[1,3] and Peng Yin[1,2]*

[1]Wyss Institute for Biologically Inspired Engineering, Harvard University, Boston, MA, USA. [2]Department of Systems Biology, Harvard Medical School, Boston, MA, USA. [3]Department of Genetics, Harvard Medical School, Boston, MA, USA. [4]Department of Biomedical Informatics, Harvard Medical School, Boston, MA, USA. [5]Image and Data Analysis Core, Harvard Medical School, Boston, MA, USA. [6]Laboratory of Systems Pharmacology, Harvard Medical School, Boston, MA, USA. [7]Media Lab, Massachusetts Institute of Technology (MIT), Cambridge, MA, USA. [8]Department of Neurobiology, Harvard Medical School, Boston, MA, USA. [9]Pathology Department, Beth Israel Deaconess Medical Center, Boston, MA, USA. [10]Present address: Department of Genome Sciences, University of Washington, Seattle, WA, USA. [11]These authors contributed equally: Sinem K. Saka, Yu Wang. *e-mail: sinem.saka@wyss.harvard.edu; yuwang01@fas.harvard.edu; py@hms.harvard.edu

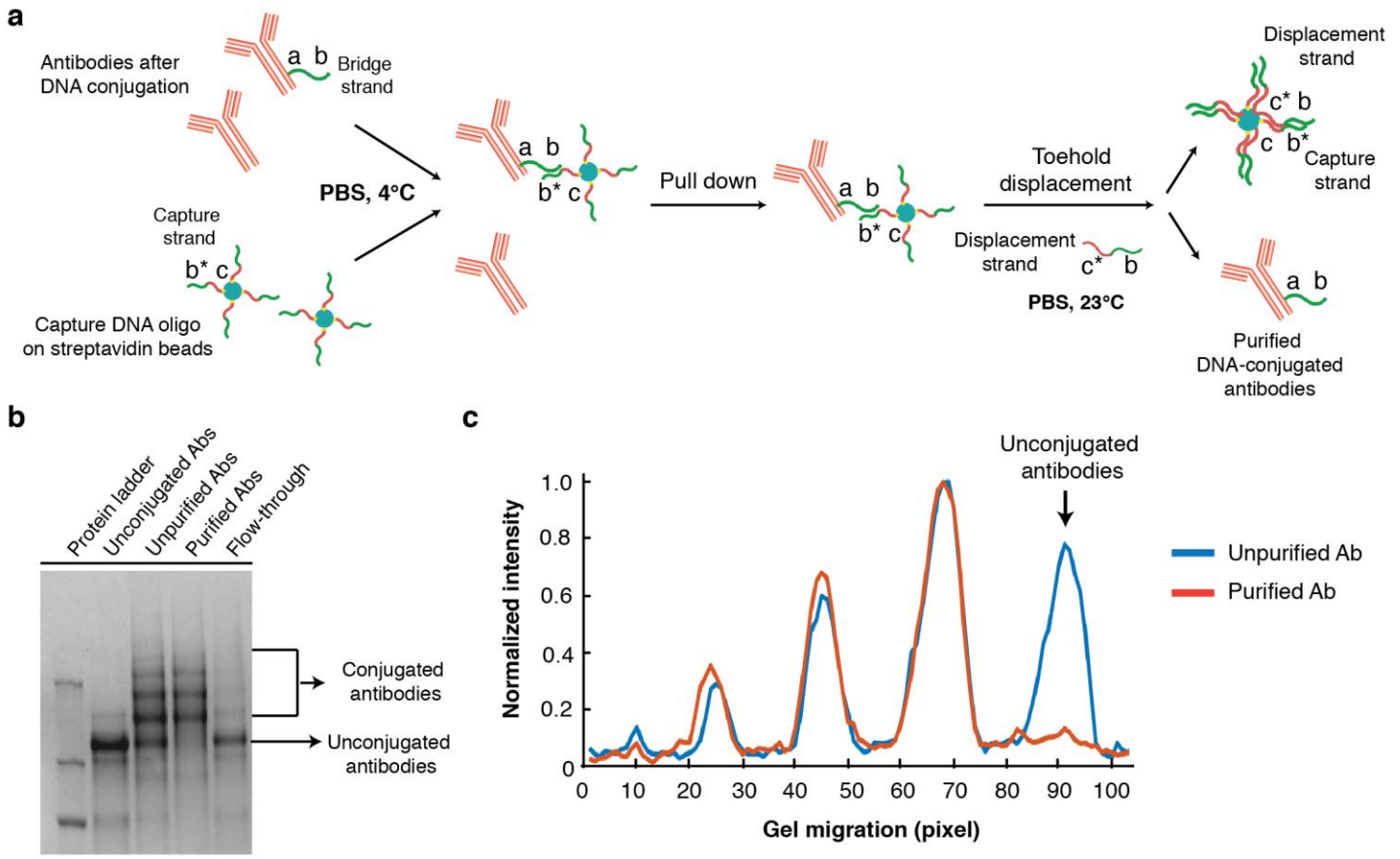

Supplementary Figure 1

Optional purification of DNA-conjugated antibodies using a toehold displacement-mediated DNA affinity pull-down.

(a) Schematic of the pull down assay. Biotin-modified capture DNA strands (biotin-*c*-*b**, where *c* is 15-nucleotides and *b** is 16-nucleotides) are attached to streptavidin beads, and used to pull down DNA-conjugated antibodies after antibody-bridge DNA conjugation (bridge strand sequence: *a*-*b,* where *b* is 16 nucleotides). The attached antibodies are dissociated from the beads using toehold displacement strands (*c**-*b*) that compete with the capture strands (Zhang and Winfree, 2009) on antibodies. While optional for Immuno-SABER, we found that purifying the DNA-conjugated antibodies via pull-down and toehold-mediated displacement may be helpful to improve the signal for select antibodies. **(b)** Visualization of purification products using an SDS-PAGE gel assay. After DNA conjugation, the majority of antibodies were conjugated with 0, 1 or 2 DNA oligos per antibody. After purification, antibodies without DNA were removed. **(c)** Plot of protein densities for the bands in **b**. The band corresponding to the removed unconjugated antibodies is marked with an arrow.

Reference: Zhang, D.Y. & Winfree, E. Control of DNA strand displacement kinetics using toehold exchange. J Am Chem Soc 131, 17303-17317 (2009).

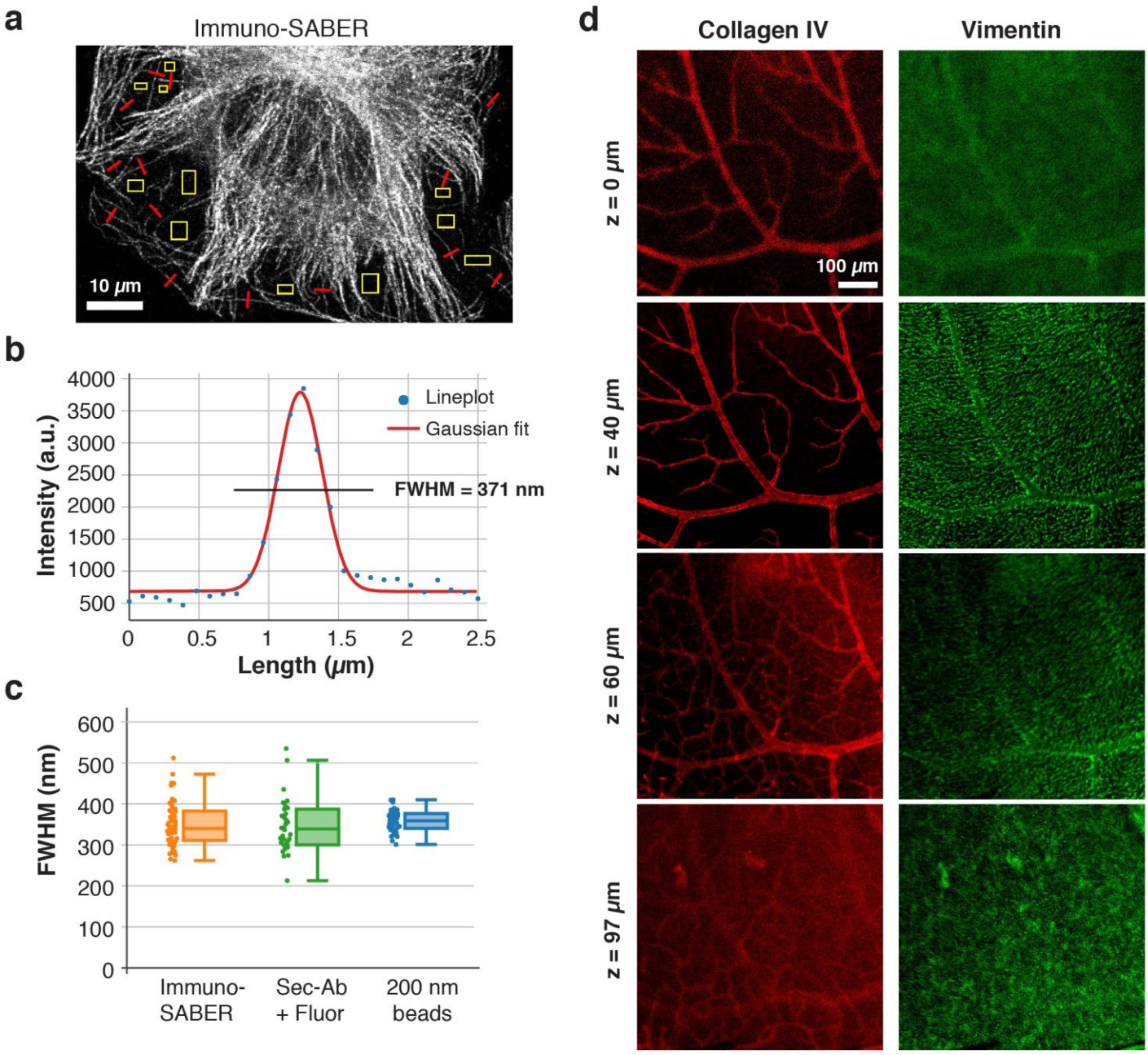

Supplementary Figure 2

Resolution and penetration controls for Immuno-SABER.

(a) ~2.5 µm long lineplots (red) were made over the thin tubules to estimate the observed resolution. Yellow-boxed background regions were used to estimate the background for subtraction. **(b)** A typical line plot along a tubule and the Gaussian fit, where full-width-half-maximum (FWHM) was calculated as 371 nm. **(c)** Mean FWHM values were calculated for 30-45 lineplots from cells stained with Immuno-SABER or fluorophore-conjugated secondary antibodies samples and the distribution was displayed as a box plot. A similar calculation was performed for 200 nm fluorescent beads. Mean FWHM was not significantly different (p value is 0.360 for Immuno-SABER and 0.335 for conventional secondary antibody staining, two-sample t-test comparison to the bead sample). Box-plots are drawn with center line, median; box limits, upper and lower quartiles; whiskers, min and max values capped at 1.5× interquartile range. **(d)** Visualization of Collagen IV and Vimentin at multiple depths of the whole mount mouse retina shown in **Fig. 2f**. Selected confocal planes are shown. Vimentin stains the Muller cells and Collagen IV stains the blood vessels, both of which are localized predominantly in the segments from nerve fiber layer to outer plexiform layer (~100 µm) of the retina (Slijkerman et al., 2015). Hence it should be noted that, although the entire whole-mount retina is about ~180 µm, the target signal comes from roughly one half of the

retina section, from the nerve fiber layer to the outer plexiform layer.

Reference: Slijkerman, R.W. et al. The pros and cons of vertebrate animal models for functional and therapeutic research on inherited retinal dystrophies. Prog Retin Eye Res 48, 137-159 (2015).

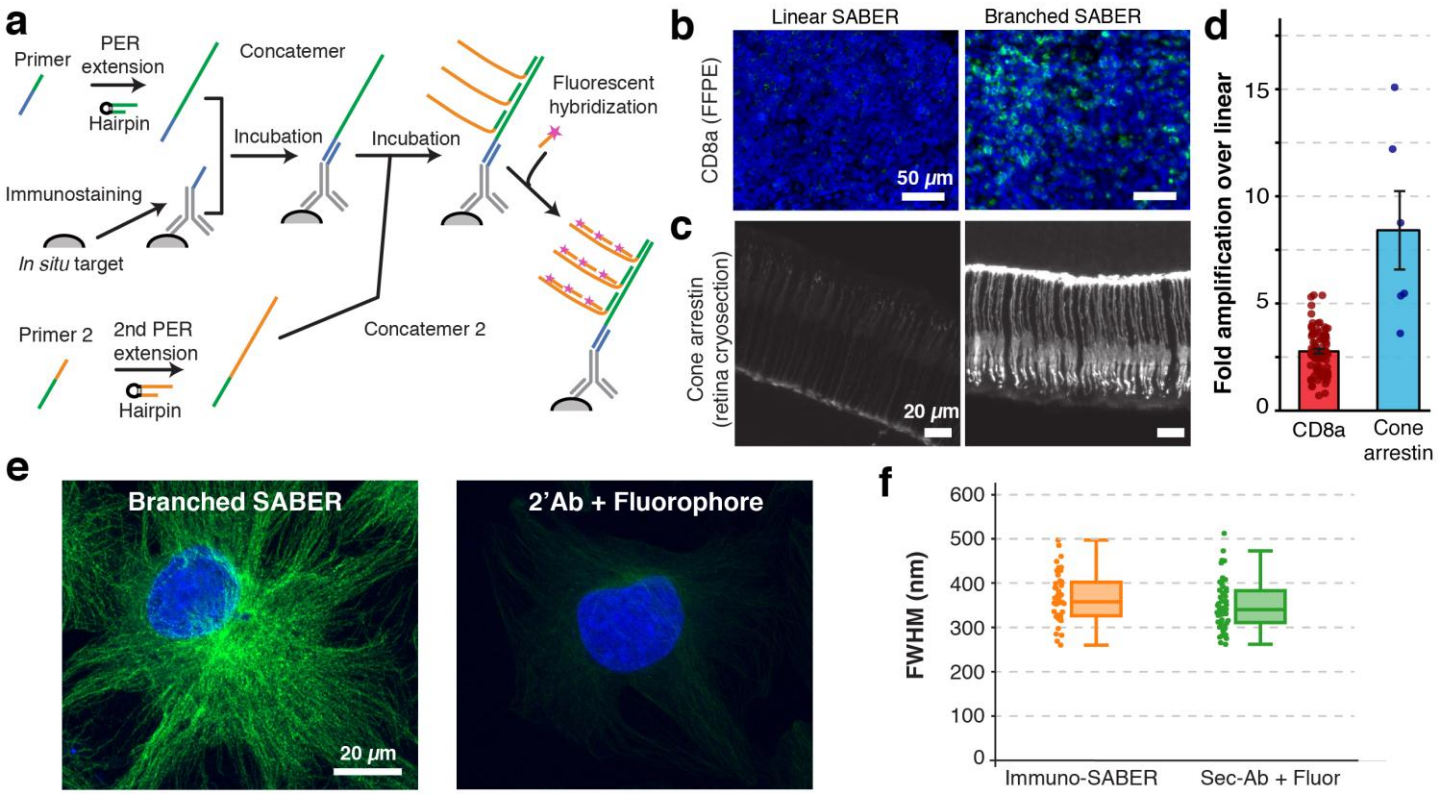

Supplementary Figure 3

Higher signal amplification via branching.

(a) Primary PER concatemers can be targeted by secondary concatemers to form a branched structure which amplifies the signal further by presenting additional binding sites for the imagers. **(b-c)** Representative images for linear and branched SABER amplification are shown for different preparations: **(b)** CD8a staining in human tonsil FFPE sections (single plane large area scans with 20× objective, cropped to show a CD8a-rich interfollicular zone region, **(c)** Cone arrestin staining in mouse retina cryosections (max projections from confocal *z* stacks). **(d)** Level of signal amplification by branched Immuno-SABER over linear was quantified by measuring the background-subtracted mean fluorescence for several regions of interest in the tissues and expressed as fold amplification over linear SABER. For CD8a FFPEs, n = 144 (for linear) and 84 (for branched) rectangular ROIs (each covering 0.03-1.20 mm^2 tissue regions; consecutive sections are used for the two conditions). For cone arrestin, n = 6 images from 2 retina samples. Error bars, s.e.m. **(e)** Alpha-tubulin staining (Alexa647) in cultured BS-C-1 cells (max projections from confocal *z* stack). **(f)** Mean FWHM values were calculated for 43 lineplots from cells stained with branched Immuno-SABER. For comparison values for conventional staining is also included. Box-plots are drawn with center line, median; box limits, upper and lower quartiles; whiskers, min and max values capped at 1.5× interquartile range. Mean FWHM for branching was not significantly different than the sub-diffraction 200 nm bead samples (plotted in **Supplementary Fig. 2c**) (p value is 0.303, two-sample t-test comparison to the bead sample).

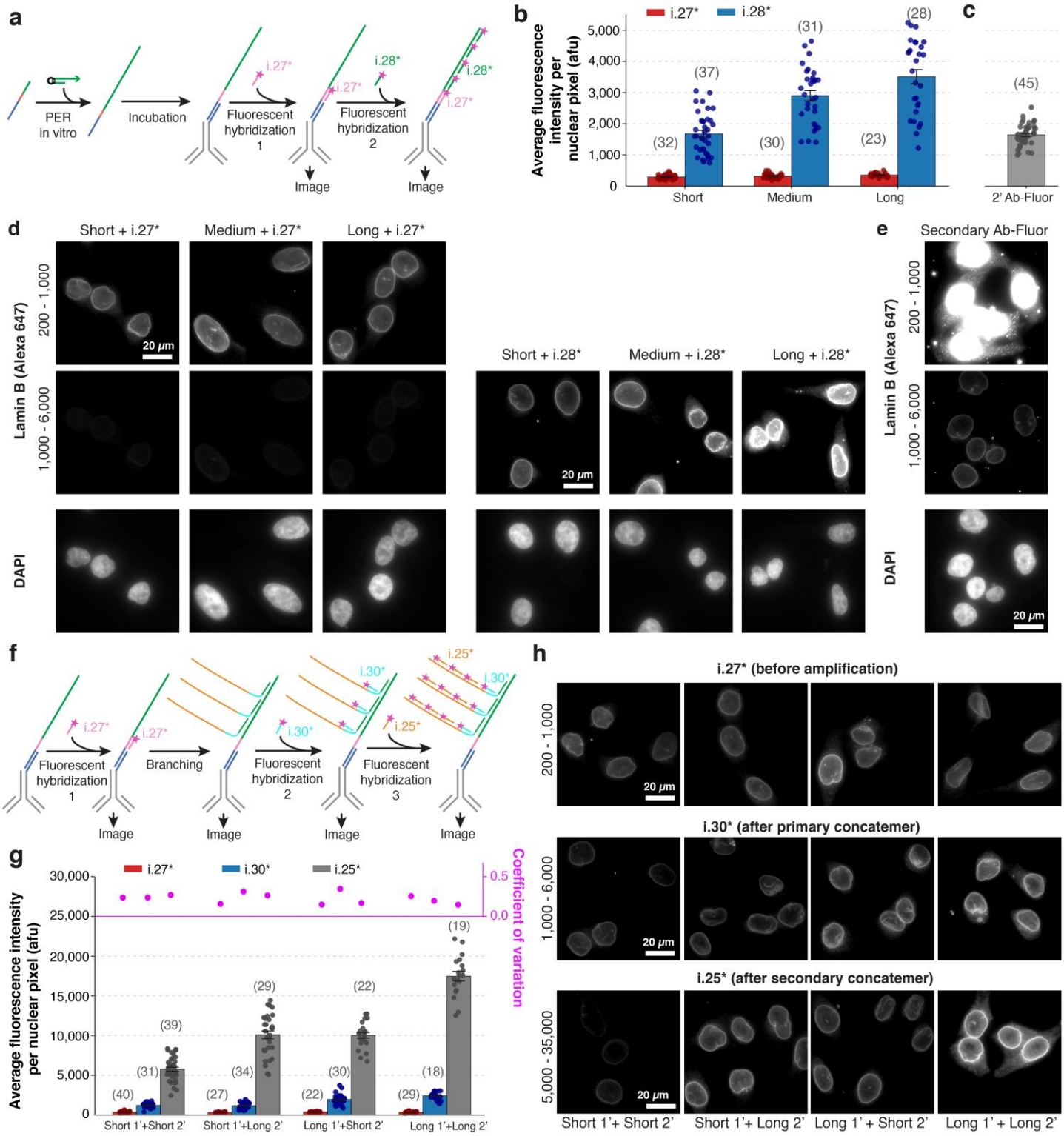

Supplementary Figure 4

Accessibility, concatemer length, and quantitativeness controls for Immuno-SABER.

(a) Experiment design: HeLa cell preparations were stained with anti-Lamin B antibodies and oligo-conjugated secondary antibodies. Concatemers of different sizes (short: 350 nt, medium: 450 nt, long: 700 nt, length estimations are based on the gel run with respect to

dsDNA ladder) were then hybridized to the antibodies. For this case, concatemers that contain an extra orthogonal binding site (for i.27*, as baseline imager) before the primer domain (p.28) were utilized. Samples were imaged first with only the baseline imager, then with the amplifier imager (i.28*). Imaging was done at 100× and 22-25 plane *z* stacks were acquired by an epifluorescence microscope. **(b)** Nuclei were segmented based on DAPI and mean Lamin B fluorescence intensity per nuclear pixel was calculated. n = 23-45 cells (individual sample sizes are written in parenthesis above each bar). Error bars, s.e.m. **(c)** For reference, the same target was also stained with commercial fluorophore-conjugated secondaries that on average bear 5× Alexa647 fluorophores and the fluorescence was measured the same way. **(d)** Representative images show the maximum projections for DAPI and Lamin B staining (Alexa647) for baseline and amplification conditions. The intensity scaling for each row is note on the left-hand side. **(e)** Secondary antibody-fluorophore images are shown for comparison. **(f)** Branching experiment design: A separate set of cells were similarly imaged with the baseline imager after hybridization of short (350 nt) or long primary concatemers (700 nt). This was followed by hybridization of secondary concatemers (short: 250 nt, long: 450 nt). Secondary concatemers also contained an orthogonal binding site (for i.30*) before the primer domain (p.25*). Baseline for branching (post-linear) was imaged by i.30*, followed by branched amplification with i.25*. **(g)** Lamin B fluorescence intensity per nuclear pixel was calculated as in **b** and is shown with the bar plot (left axis) overlaid with the scatter plot showing the distribution in the dataset. The dot plot above (magenta, right axis) shows the coefficient of variation for all the conditions. Note that the imagers bind dimers of primer units, whereas branches bind trimers for higher stability during exchange rounds. Therefore compared to the i.28* staining in previous panels, i.30* is expected to yield 1.5-fold lower signal (blue bars in **b** and **g**). **(h)** Representative images show the maximum projections corresponding to the conditions in **g**. All images are acquired under comparable conditions, and are displayed at the given intensity scaling for each amplification level.

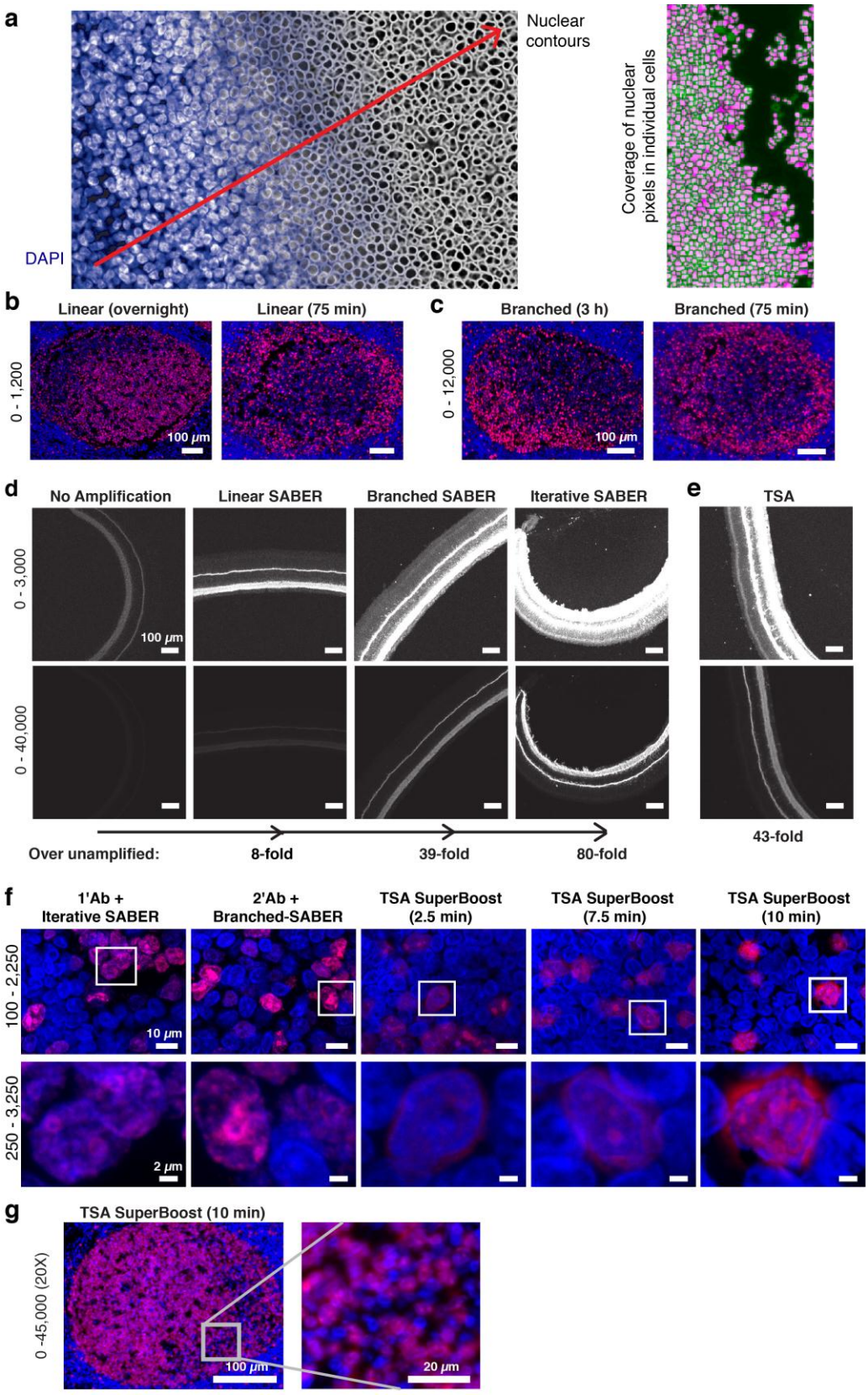

Supplementary Figure 5

Additional images for branching.

(a) Machine-learning based nucleus segmentation for signal quantification: The deep learning model was trained with a manually annotated dataset to enable automatic identification of nuclear contours to be followed by watershed segmentation. The image highlights nuclear contours (right side of the image) from DAPI staining (left side). Right panel: Watershed segmentation was used to segment (pink) the pixels corresponding to nuclei of each cell**. (b-c)** Images display a typical germinal center in human FFPE tonsil samples stained for Ki-67 (Alexa647, red) by Immuno-SABER. DAPI stain (blue) is shown for reference. Qualitatively similar amplification levels were obtained by long and short hybridization times (at 37°C) for the primary concatemer and branching concatemer (75 min each). **(d)** Iterative SABER of SV2 (Alexa647) in a 40 μm mouse retina cryosection. **(e)** For comparison SV2 staining with TSA was performed using mono HRP conjugated secondary antibodies. **(f)** Zoom-out and zoom-in views of the high-magnification confocal images in **Fig. 3f** displayed at different scaling ranges for comparative visualization. 10 min TSA amplification is included for further comparison. **(g)** Application of tyramide-Alexa647 for the maximum recommended incubation of 10 min. The germinal center image on the left is scaled in the same range with **Fig. 3d**. Zoom-in on the right is included to display the significant blurring of the signal at 10 min incubation.

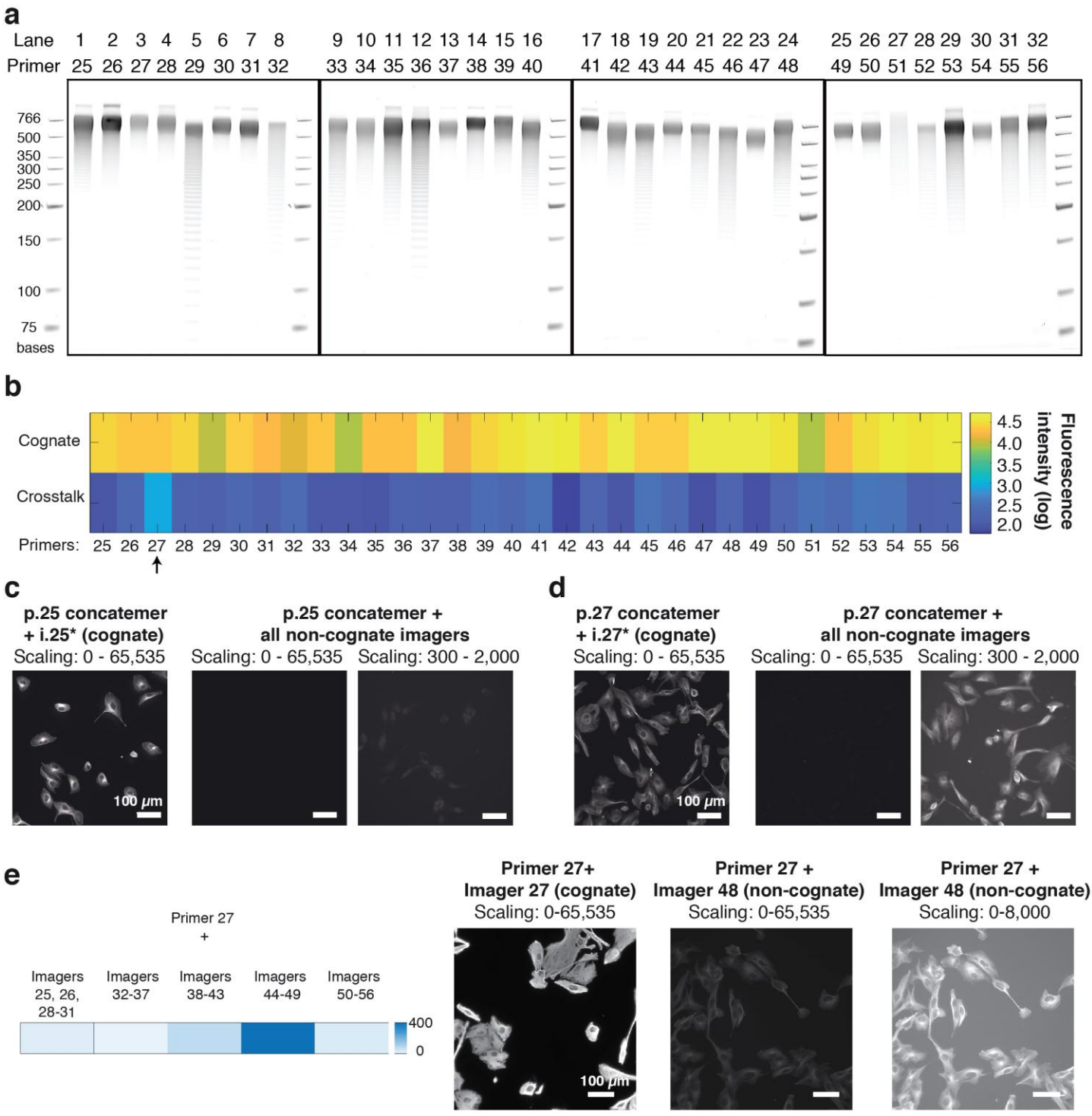

Supplementary Figure 6

Sequence validation for Exchange-SABER.

(a) 32 SABER sequences were extended to ~650 bases *in vitro* and examined by gel shift assay visualized with SybrGold on 6% denaturing PAGE gels. Qualitatively, 18 of the 32 sequences (such as #29) displayed a broader distribution with a ladder of shorter products visible albeit these bands being much dimmer than the predominant concatemer band. Although being extended, one sequence (#51) had a more even distribution in the upper length regime without a clear predominant band. Based on these

distributions, particular applications may favor a subset of the sequence library, i.e. high efficiency primers (for example primers 27, 28, 30, 31, 37, 38, 41, 44, 47, 49, 50, 54) may be more favorably utilized for more quantitative experiments or for lower abundance proteins. **(b-d)** *In situ* performance and crosstalk analysis. BS-C-1 cells were stained with bridge DNA-conjugated antibodies targeting α-Tubulin on a 96-well plate. Concatemers extended from each primer were hybridized to the bridges creating an array of wells labeled with primer sequences p.25-p.56. For each concatemer two sets of wells were prepared: (i) cognate group to be incubated with the corresponding imager strands, and (ii) crosstalk group where we added mixtures of imagers except the cognate imager strand. For each primer (e.g. p.25), both cognate and crosstalk wells were prepared by either applying the corresponding Alexa647-imager (e.g. i.25*) or all the imagers except the cognate one (e.g. -i.26* to i.56*). Images were captured in 16-bit (0-65,535). Representative images are shown for Primer 25 (p.25) **(c)** and Primer 27 (p.27) concatemers **(d)**. Crosstalk images are displayed with two different intensity scales to render the crosstalk signal visible. The fluorescence signals were quantified and plotted in the log scale and displayed as a heatmap. Consistent with the *in vitro* gel shift assay in panel **a**, sequences that had lower extension efficiency (particularly primers 29, 32, and 51) tended to yield less fluorescence signal compared to sequences that that extend with higher efficiency. Non-negligible crosstalk signal was only detected for Primer 27 concatemer (red box). **(e)** Crosstalk analysis of primer sequence p.27. BS-C-1 cells were fixed and stained with DNA-conjugated antibodies targeting alpha-Tubulin. Concatemers extended from primer sequence p.27 were hybridized to the antibodies, followed by addition of non-cognate imager strands. We first grouped every five imager strands and determined that p.27 had crosstalk with imager 44-49. We then tested individual imager strands from imager 44-49 and determined the strand responsible for crosstalk as imager strand 48 (i.48*), which is excluded from the library for further multiplexed imaging in presence of p.27.

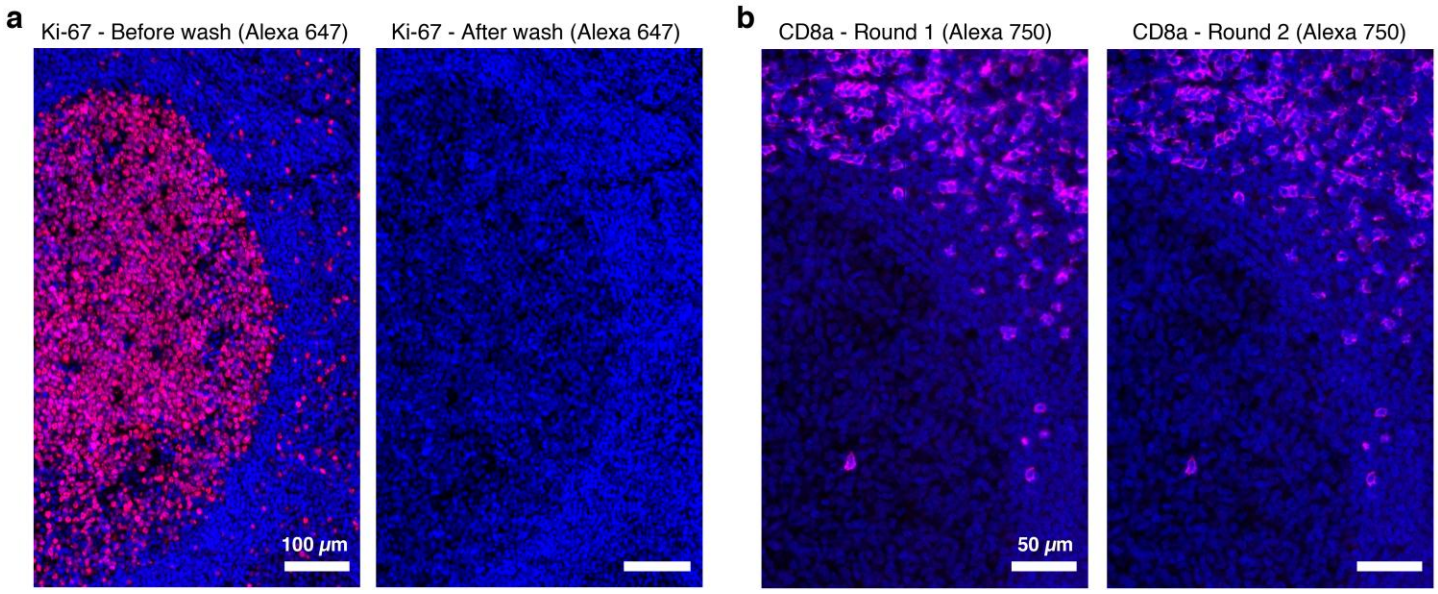

Supplementary Figure 7

Controls for exchange imaging of FFPE human tonsil sections.

(a) Imagers can efficiently removed within 10 min by washing the sample with 50% formamide in PBS, as shown in before and after wash images of the same section stained for Ki-67 (red) with linear amplification, imaged and displayed under the same conditions. DAPI stain is shown in blue. **(b)** Under this wash condition (10 min with 50% formamide in PBS at RT) the concatemers are not displaced, as shown by exchange imaging of CD8a by re-binding the imagers to the same target and re-imaging the tissue section (linear amplification).

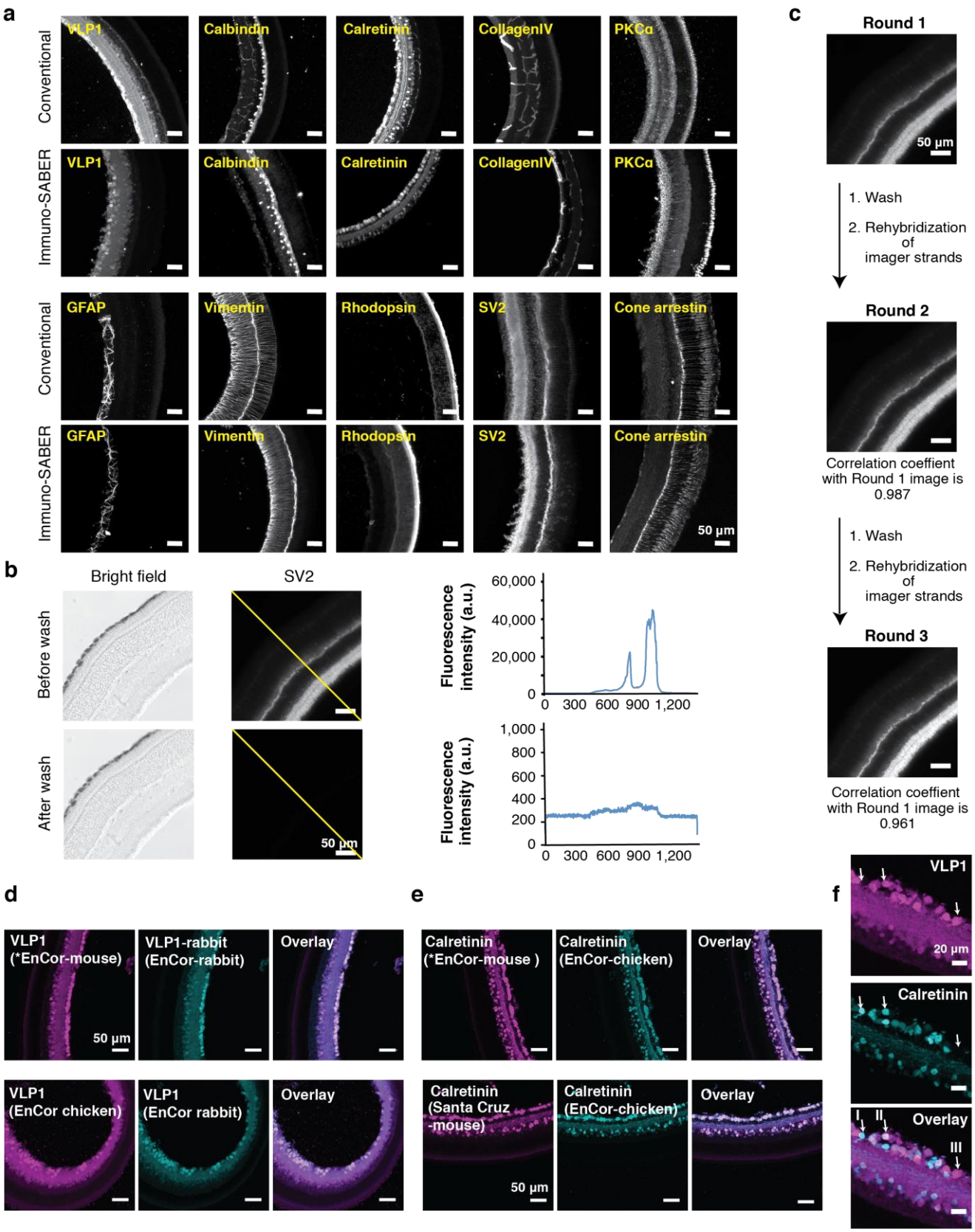

Supplementary Figure 8

Control experiments for highly multiplexed imaging in mouse retina sections.

(a) Comparison of antibody staining patterns before and after DNA conjugation. The images for unconjugated antibodies were taken using conventional fluorophore-conjugated secondary antibody labeling, and the images for antibodies after conjugation were taken using primary antibody-Immuno SABER labeling (images are displayed at individual contrast levels). **(b)** Efficiency of washing to remove the imager strands. A 30 μm mouse retina section was stained with DNA-conjugated SV2 antibodies and imaged using Alexa647-i.26* imager with a widefield microscope. Imager strands were washed using 0.1× PBS with 30% formamide at room temperature for 3×10 min. Before and after images were taken using the same imaging setting. The fluorescence intensity of indicated yellow line was measured using FIJI. **(c)** Washing conditions maintained sample integrity without signal loss. SV2 in mouse retina sections was imaged for 3 rounds and the correlation coefficient was calculated. The correlation coefficient between the images was above 0.95, suggesting the washing condition is sufficiently mild and non-disruptive. **(d-e)** Validation of the VLP1 and calretinin antibodies with conventional indirect immunostaining: The VLP1 (EnCor-mouse) and calretinin (EnCor-mouse) that were used for the multiplexing experiments (marked with asterisk) in **Fig. 5** were tested for specificity by co-staining with other antibodies targeting the same targets, followed by visualization using fluorophore-conjugated secondary antibodies. **(f)** Three cell subtypes (marked with arrows, I: $VLP1^{+}$ and $Calretinin^{+}$, II: $VLP1^{-}$ and $Calretinin^{+}$, III: $VLP1^{+}$ and $Calretinin^{-}$) identified in the multiplexed mouse retina imaging experiment were verified using conventional immunostaining with unconjugated primary antibodies (VLP1 by EnCor-rabbit and Calretinin by EnCor-mouse) and fluorophore-conjugated secondary antibodies.

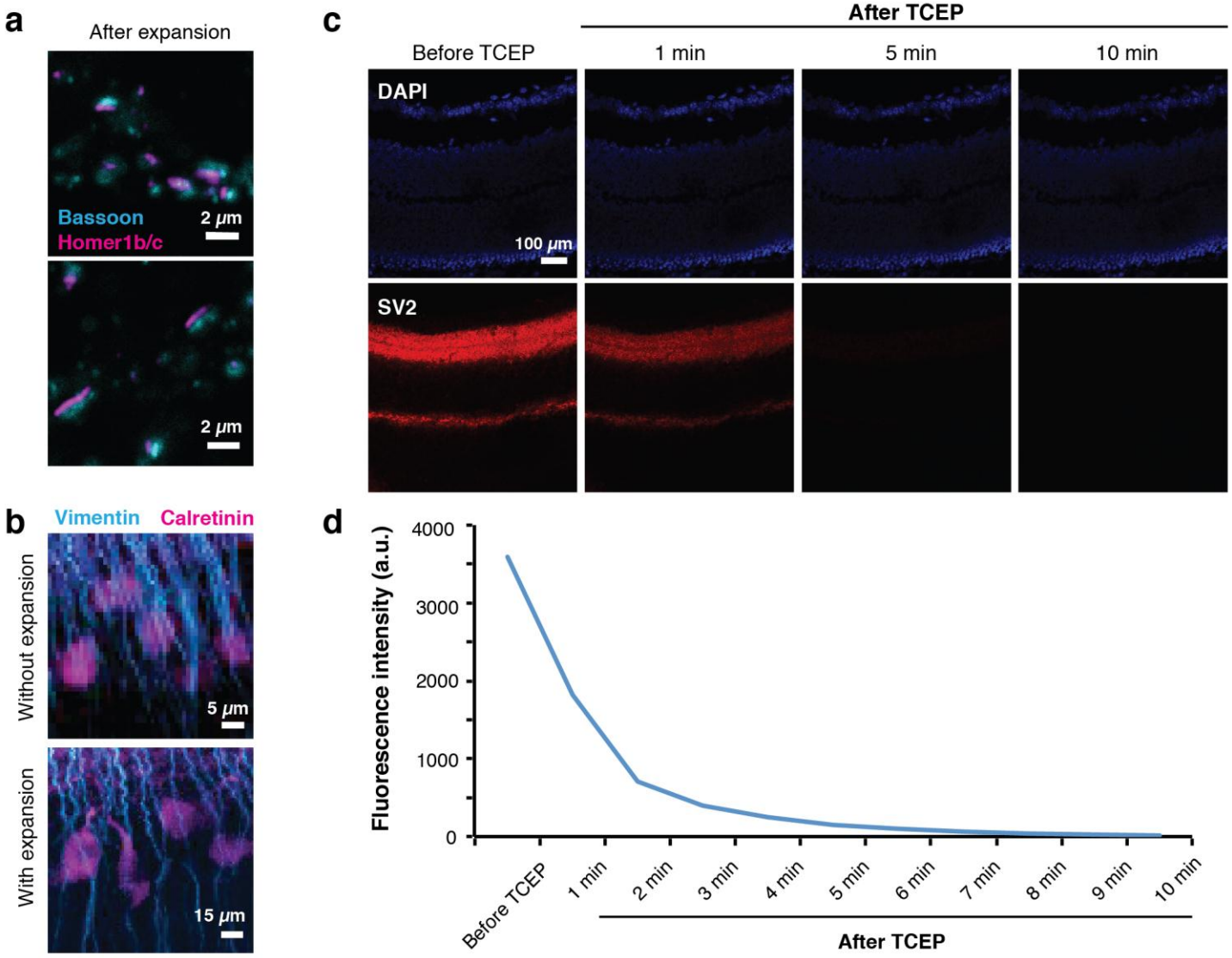

Supplementary Figure 9

Other sample orientations and alternative reduction-mediated fluorophore removal timeline for Expansion-SABER.

(a) Additional post-expansion images of neuronal synapses showing different orientations, as in **Fig. 6b**. **(b)** High-zoom comparison of Vimentin and Calretinin signals with and without expansion. The image with expansion is the overlay of the Vimentin and Calretinin images from **Fig. 6c**, whereas the image without expansion was derived from images in **Fig. 5a**. Scale bar indicates the physical size after expansion (~3-fold). **(c)** Alternative fluorophore removal strategy using TCEP reduction in thick expanded samples using TCEP. A mouse retina section stained with SV2 was expanded and visualized with disulfide bond modified imager strands. The fluorophores (Alexa 647) on the imager strands were cleaved using TCEP reduction. The fluorescence signal was monitored using a confocal microscope in a time course for 10 min. **(d)** Quantification of fluorescence signals in **c** before and after TCEP reduction.

Supplementary Tables

Supplementary Table 1. Optimized concatemer extension conditions and sequences for the primer library (for Supplementary Fig. 6).

Primer ID	Primer sequence	Hairpin ID	Hairpin sequence	Hairpin concentration	Time
p.25	CCAATAATA	h.25.25	ACCAATAATAGGGCCTTTTGGCCCTATTATT GGTTATTATTGG/3InvdT/	0.15 μM	3 h
p.26	ATAAACCTA	h.26.26	AATAAACCTAGGGCCTTTTGGCCCTAGGTTT ATTTAGGTTTAT/3InvdT/	0.9 μM	3 h
p.27	CATCATCAT	h.27.27	ACATCATCATGGGCCTTTTGGCCCATGATG ATGTATGATGATG/3InvdT/	0.075 μM	3 h
p.28	CAACTTAAC	h.28.28	ACAACTTAACGGGCCTTTTGGCCCGTTAAG TTGTGTTAAGTTG/3InvdT/	0.3 μM	2 h
p.29	TCTAAAATC	h.29.29	ATCTAAAATCGGGCCTTTTGGCCCGATTTTA GATGATTTTAGA/3InvdT/	0.15 μM	3 h
p.30	AATACTCTC	h.30.30	AAATACTCTCGGGCCTTTTGGCCCGAGAGT ATTTGAGAGTATT/3InvdT/	0.5 μM	2 h
p.31	TTATTCACT	h.31.31	ATTATTCACTGGGCCTTTTGGCCCAGTGAAT AATAGTGAATAA/3InvdT/	0.85 μM	2 h
p.32	CTTTTTTTC	h.32.32	ACTTTTTTTCGGGCCTTTTGGCCCGAAAAAA AGTGAAAAAAAG/3InvdT/	1.5 μM	3 h
p.33	CCTTCTATT	h.33.33	ACCTTCTATTGGGCCTTTTGGCCCAATAGAA GGTAATAGAAGG/3InvdT/	0.5 μM	2 h
p.34	CTCTACTAC	h.34.34	ACTCTACTACGGGCCTTTTGGCCCGTAGTAG AGTGTAGTAGAG/3InvdT/	0.4 μM	2 h
p.35	TAAAAACTC	h.35.35	ATAAAAACTCGGGCCTTTTGGCCCGAGTTTT TATGAGTTTTTA/3InvdT/	1.5 μM	3 h
p.36	AACTAATCT	h.36.36	AAACTAATCTGGGCCTTTTGGCCCAGATTA GTTTAGATTAGTT/3InvdT/	1 μM	2 h
p.37	TTTCTCTTC	h.37.37	ATTTCTCTTCGGGCCTTTTGGCCCGAAGAGA AATGAAGAGAAA/3InvdT/	0.85 μM	2 h
p.38	AACATACTA	h.38.38	AAACATACTAGGGCCTTTTGGCCCTAGTAT GTTTTAGTATGTT/3InvdT/	0.5 μM	2 h
p.39	TTCATTTAC	h.39.39	ATTCATTTACGGGCCTTTTGGCCCGTAAATG AATGTAAATGAA/3InvdT/	1 μM	2 h
p.40	ATCCTACAA	h.40.40	AATCCTACAAGGGCCTTTTGGCCCTTGTAG GATTTTGTAGGAT/3InvdT/	0.9 μM	2 h
p.41	CAATCAAAA	h.41.41	ACAATCAAAAGGGCCTTTTGGCCCTTTTGAT TGTTTTTGATTG/3InvdT/	0.45 μM	3 h
p.42	CTTACAAAC	h.42.42	ACTTACAAACGGGCCTTTTGGCCCGTTTGTA AGTGTTTGTAAG/3InvdT/	0.5 μM	2 h
p.43	ACAAATAAC	h.43.43	AACAAATAACGGGCCTTTTGGCCCGTTATTT GTTGTTATTTGT/3InvdT/	0.5 μM	2 h
p.44	TTTTCTACC	h.44.44	ATTTTCTACCGGGCCTTTTGGCCCGGTAGAA AATGGTAGAAAA/3InvdT/	0.45 μm	3h
p.45	CCCTTATTT	h.45.45	ACCCTTATTTGGGCCTTTTGGCCCAAATAAG GGTAAATAAGGG/3InvdT/	0.4 μM	3 h
p.46	TCTTTCATT	h.46.46	ATCTTTCATTGGGCCTTTTGGCCCAATGAAA GATAATGAAAGA/3InvdT/	0.45 μM	3 h
p.47	TTCTTACTC	h.47.47	ATTCTTACTCGGGCCTTTTGGCCCGAGTAAG AATGAGTAAGAA/3InvdT/	0.85 μM	1 h
p.48	CCATAAATC	h.48.48	ACCATAAATCGGGCCTTTTGGCCCGATTTAT GGTGATTTATGG/3InvdT/	0.4 μM	3 h

p.49	CATTTATCC	h.49.49	ACATTTATCCGGGCCTTTTGGCCCGGATAA ATGTGGATAAATG/3InvdT/	0.65 µM	1 h
p.50	ATACTTCAC	h.50.50	AATACTTCACGGGCCTTTTGGCCCGTGAAG TATTGTGAAGTAT/3InvdT/	0.4 µM	1 h
p.51	TACCTCTAA	h.51.51	ATACCTCTAAGGGCCTTTTGGCCCTTAGAG GTATTTAGAGGTA/3InvdT/	0.6 µM	3 h
p.52	CTCCTATTT	h.52.52	ACTCCTATTTGGGCCTTTTGGCCCAAATAGG AGTAAATAGGAG/3InvdT/	0.3 µM	2 h
p.53	CTATCCAAA	h.53.53	ACTATCCAAAGGGCCTTTTGGCCCTTTGGAT AGTTTTGGATAG/3InvdT/	0.2 µM	3 h
p.54	ATCCCTATC	h.54.54	AATCCCTATCGGGCCTTTTGGCCCGATAGG GATTGATAGGGAT/3InvdT/	0.1 µM	3 h
p.55	TCATTACTT	h.55.55	ATCATTACTTGGGCCTTTTGGCCCAAGTAAT GATAAGTAATGA/3InvdT/	0.65 µM	3 h
p.56	CTAAATCTC	h.56.56	ACTAAATCTCGGGCCTTTTGGCCCGAGATTT AGTGAGATTTAG/3InvdT/	0.35 µM	3 h
Test-primer[29]	TCTCTTATT	h.test	ATCTCTTATTGGGCCTTTTGGCCCAATAAGA GATAATAAGAGA/3InvdT/	Not included in the gel assay	

The full set of 50 designed primer sequences are available in our recent work[30].

Supplementary Table 2. Bridge sequences used for antibody conjugation.

Bridge sequence index	DNA sequence
bc42_0	AATTCTATGACACCGCCACGCCCTATATCCTCGCAATAACCC
bc42_1	ATTATCCCTACCGCCAAATCTCCGTGTCCTTAACCGACCTAT
bc42_2	CGTTATCGCCGCCTTATCCACTGTACGATCCTATTCCTCTCC
bc42_3	GTTTCCTATATTTAGCGTCCGTGTCGTTCTCCCGCGCAACAG
bc42_4	TATCTTAAGTCTTCGCGTGTTGTCTCGTCTGGGTATTGCGTT
bc42_5	TCCTGTCCCGACGATCCTACCCTTAAAGTTACTGCGCACCCT
bc42_6	CGGTGAGGTAGGAGTCGTGCGTATCGTTTCCTATATAGCCGT
bc42_7	AGTTCCTGTAGTATCCCGTCGCATAGTCGTACATTCACCGTC
bc42_8	AACAATTCAGCTCCGCCTTATACCGTCTTACCGCCAACATCG
bc42_9	GAATTTGGCCCGTTCTATGTCTAACTCGTGTTCCCGCTTGTA
bc42_10	GTCCTCGCTCTTTCCGCATTTTCCCGTATGCGCTTTGTATTA
bc42_11	TGTCTAAATTCTAATGCCGCCCTATGCCGCCGTTCCAACAAT
bc42_12	CCTTCCGCCGTATGAATTTGACCCGAAGCCCAACCCGACCCT
bc42_13	CAGTTCTTGTATCGCGTCACTTATCGGTTATTGTCCTCTCGC
bc42_14	CCAACCTCTCGTACCAAATTCCGCCACTCAAGCCGTATCAAA
bc42_15	GTTTCAAGAGTCCGTCGCAAATTCCACTACACGCTACGCCCA
25mer-tester	TATTTAGTGTTCGAATAGTTCGATCTAG

The full set of 84 designed bridge sequences are available in our recent work[30]. For conjugation bridge oligos are designed as follows: /5ThioMC6-D/ tt (linker) bridge sequence (42mer).

Supplementary Table 3. Imager strands used for fluorescent visualization.

Imager ID	Imager sequence
i.25*	/Fluorophore/tt-TATTATTGG-t -ATTATTGG-t /3InvdT/
i.26*	/Fluorophore/tt-TAGGTTTAT-t-TAGGTTTAT-t /3InvdT/
i.27*	/Fluorophore/ tt-ATGATGATG-t-ATGATGATG-t 3InvdT/
i.28*	/Fluorophore/ tt-GTTAAGTTG-t-GTTAAGTTG-t/3InvdT/
i.29*	/Fluorophore/ tt-GATTTTAGA-t-GATTTTAGA-t/3InvdT/
i.30*	/Fluorophore/ tt-GAGAGTATT-t-GAGAGTATT-t/3InvdT/
i.31*	/Fluorophore/ tt-AGTGAATAA-t-AGTGAATAA-t/3InvdT/
i.32*	/Fluorophore/ tt-GAAAAAAAG-t-GAAAAAAAG-t/3InvdT/
i.33*	/Fluorophore/ tt AATAGAAGGt AATAGAAGG-t /3InvdT/
i.34*	/Fluorophore/ tt-GTAGTAGAG-t-GTAGTAGAG-t /3InvdT/
i.35*	/Fluorophore/ tt-GAGTTTTTA-t-GAGTTTTTA-t /3InvdT/
i.36*	/Fluorophore/ tt-AGATTAGTT-t-AGATTAGTT-t /3InvdT/
i.37*	/Fluorophore/ tt-GAAGAGAAA-t-GAAGAGAAA-t /3InvdT/
i.38*	/Fluorophore/ tt-TAGTATGTT-t-TAGTATGTT-t /3InvdT/
i.39*	/Fluorophore/ tt-GTAAATGAA-t-GTAAATGAA-t /3InvdT/
i.40*	/Fluorophore/ tt-TTGTAGGAT-t-TTGTAGGAT-t /3InvdT/
i.41*	/Fluorophore/ tt-TTTTGATTG-t-TTTTGATTG-t /3InvdT/
i.42*	/Fluorophore/ tt-GTTTGTAAG-t-GTTTGTAAG-t /3InvdT/
i.43*	/Fluorophore/ tt-GTTATTTGT-t-GTTATTTGT-t /3InvdT/
i.44*	/Fluorophore/ tt-GGTAGAAAA-t-GGTAGAAAA-t /3InvdT/
i.45*	/Fluorophore/ tt-AAATAAGGG-t-AAATAAGGG-t /3InvdT/
i.46*	/Fluorophore/ tt-AATGAAAGA-t-AATGAAAGA-t /3InvdT/
i.47*	/Fluorophore/ tt-GAGTAAGAA-t-GAGTAAGAA-t /3InvdT/
i.48*	/Fluorophore/ tt-GATTTATGG-t-GATTTATGG-t /3InvdT/
i.49*	/Fluorophore/ tt-GGATAAATG-t-GGATAAATG t /3InvdT/
i.50*	/Fluorophore/ tt-GTGAAGTAT-t-GTGAAGTAT t /3InvdT/
i.51*	/Fluorophore/ tt-TTAGAGGTA-t-TTAGAGGTA-t /3InvdT/
i.52*	/Fluorophore/ tt-AAATAGGAG-t-AAATAGGAG-t /3InvdT/
i.53*	/Fluorophore/ tt-TTTGGATAG-t-TTGGATAG-t /3InvdT/
i.54*	/Fluorophore/ tt-GATAGGGAT-t-GATAGGGAT-t /3InvdT/
i.55*	/Fluorophore/ tt AAGTAATGA-t-AAGTAATGA t /3InvdT/
i.56*	/Fluorophore/ tt GAGATTTAG-t-GAGATTTAG t /3InvdT/
Test-imager	/Fluorophore/ tt-AATAAGAGA-t-AATAAGAGA-t /3InvdT/

Supplementary Table 4. Antibodies used in SABER experiments, conjugated bridge sequences and respective SABER primers.

Antibody target	Source	Bridge sequence (for conjugation)	Capture and Toehold sequences for purification (if purified)	SABER primer sequences used in the experiments (+ denotes branching)
Cone arrestin	Millipore #AB15282	25mer-tester	Capture: Biotin-GTTGCTGTCGTATGT-CTAGATCGAACTATTC Toehold: GAATAGTTCGATCTAG-ACATACGACAGCAAC	p.30 (Fig. 2) or p28 + p25 (Supplementary Fig. 3) or test-primer (Fig. 5)
GFAP	ThermoFisher #13-0300	bc42_1	Capture: Biotin - GGGTAGGGTAGTGGT-ATAGGTCGGTTAAGGA Toehold: TCCTTAACCGACCTAT-ACCACTACCCTACCC	p.36 (Fig. 5 and 6)
PKCα	Novus #NB600-201	bc42_2	Binding sequence: Biotin - CGAGTGAGGTGGAAT-GGAGAGGAATAGGATC Toehold sequence: GATCCTATTCCTCTCC-ATTCCACCTCACTCG	p.25 (Fig. 5)
SV2	HybridomaBank Antibody Registry ID: AB_2315387	bc42_3	Capture: Biotin - CGAGTGGTAAGGCAT-CTGTTGCGCGGGAGAA Toehold: TTCTCCCGCGCAACAG-ATGCCTTACCACTCG	p.26 (Fig. 5, 6, Supplementary Fig. 8-9); or p27 + p28 + p32 (Supplementary Fig. 3)
Collagen IV	Novus #NB120-6586	bc42_4	Capture: Biotin - GAAATAGAATGAACG-AACGCAATACCCAGAC Toehold: GTCTGGGTATTGCGTT-CGTTCATTCTATTTC	p.27 (Fig. 2, 5 and 6)
Rhodopsin	EnCor Bio #MCA-A531	bc42_7	Capture: Biotin - GTTAAGGTGGAATGA-GACGGTGAATGTACGA Toehold: TCGTACATTCACCGTC-TCATTCCACCTTAAC	p.33 (Fig. 5 and 6)
Calbindin	EnCor Bio #MCA-5A9	bc42_8	Capture: Biotin - GGTGAGGTGTAGTGG-CGATGTTGGCGGTAAG Toehold: CTTACCGCCAACATCG-CCACTACACCTCACC	p.34 (Fig. 5)
Vimentin	Cell Signaling #5741S	bc42_9	Capture: Biotin - CGGAACAGATAAAGA-TACAAGCGGGAACACG Toehold: CGTGTTCCCGCTTGTA-TCTTTATCTGTTCCG	p.28 (Fig. 2. 5 and 6)
Calretinin	EnCor Bio #MCA3G9	bc42_10	Capture: Biotin - GCCAAATTCCACCGC-TAATACAAAGCGCATA Toehold: TATGCGCTTTGTATTA-GCGGTGGAATTTGGC	p.30 (Fig. 5 and 6)
VLP1	EnCor Bio #MCA-2D11	bc42_11	Capture: Biotin - CGGATGATGAGGGTG-ATTGTTGGAACGGCGG Toehold: CCGCCGTTCCAACAA-TCACCCTCATCATCCG	p.39 (Fig. 5)
Alpha-Tubulin	ThermoFisher #MA1-80017	bc42_0	Capture: Biotin - GTTGAGTGAGGTTGA-GGGTTATTGCGAGGAT Toehold: ATCCTCGCAATAACCC-TCAACCTCACTCAAC	p.30 or p.30 + p.28
Ki-67	Cell Signaling #9129 (formulated in PBS)	bc42_1	Capture: Biotin - GGGTAGGGTAGTGGT-ATAGGTCGGTTAAGGA Toehold: TCCTTAACCGACCTAT-ACCACTACCCTACCC	p.41 + p.34 (Fig. 4c), or p.30 or p.30 + p.28 or p.30 + p.28 + p.25 (all other figures)
CD8a	Cell Signaling	bc42_2	Capture: Biotin - CGAGTGAGGTGGAAT-	p.40 + p.28 (Fig. 4c) or

	#85336 (formulated in PBS)		GGAGAGGAATAGGATC Toehold: GATCCTATTCCTCTCC-ATTCCACCTCACTCG	p.25 + p.31 (all other figures)
PD-1	Cell Signaling #43248 (formulated in PBS)	bc42_3	Capture: Biotin - CGAGTGGTAAGGCAT-CTGTTGCGCGGGAGAA Toehold: TTCTCCCGCGCAACAG-ATGCCTTACCACTCG	p.26 + p.39
IgA	Jackson #109-005-011	bc42_7	Unpurified	p.34 (Fig. 4a) or p.25 (Fig. 4c)
CD3e	Cell Signaling #85061 (formulated in PBS)	bc42_9	Capture: Biotin - CGGAACAGATAAAGA-TACAAGCGGGAACACG Toehold: CGTGTTCCCGCTTGTA-TCTTTATCTGTTCCG	p.27 + p.32
IgM	Jackson #709-006-073	bc42_11	Unpurified	p.39 (Fig. 4a) or p.35 (Fig. 4c)
Lamin B	Santa Cruz sc-6216	25mer-tester (conjugated onto anti-goat secondary antibody, Jackson ImmunoResearch # 705-005-147)	Unpurified	p.28 + p.25 (Supplementary Fig. 6)
Bassoon	Enzo ADI-VAM-#PS003	bc42_0 (conjugated onto anti-mouse secondary antibody, Jackson ImmunoResearch #715-005-151)	Unpurified	p.30 (Fig.6 and Supplementary Fig. 9)
Homer1b/c	ThermoFisher #PA5-21487	bc42_3 (conjugated onto anti-rabbit secondary antibody, Jackson ImmunoResearch #711-005-152)	Unpurified	p.26 (Fig. 6 and Supplementary Fig. 9)
Anti-rabbit IgG (to detect Ki-67 indirectly)	Jackson # 711-005-152	bc42_3	Unpurified	p.30 + p.28 (Fig. 3d-f, Supplementary Fig. 5f)

Antibodies used to validate colocalization of VLP1 and Calretinin in **Supplementary Fig. 8d-f** are Calretinin (SantaCruz #SC-365956; EnCor Bio #CPCA-Calret; EnCor Bio #MCA-3G9 AP), VLP1 (EnCor Bio #RPCA-VLP1; EnCor Bio #CPCA-VLP1; EnCor Bio #MCA-2D11).
Fluorophore-conjugated secondary antibodies used for reference imaging: anti-rat-Alexa647 (Thermo Fisher #A-21472), anti-rabbit-Alexa488 (Thermo Fisher #A-21206), anti-rabbit-Atto488 (Rockland #611-152-122S), anti-mouse-Alexa647 (Thermo Fisher #A-31571), anti-goat-Alexa647 (Thermo Fisher # A-21447), anti-rabbit-Alexa647 (Jackson ImmunoResearch, 711-605-152).

Supplementary Table 5. Quantification strands.

Sequence ID	Sequence	Experiment / Figure number
25mer-tester*-tt-p.28-a-p.28	CTAGATCGAACTATTCGAACACTAAATA-tt-CAACTTAAC-a-CAACTTAAC	SABER for cone arrestin - unamplified control (Fig. 2 and Supplementary Fig. 3)
25mer-tester*-tt-p.28	CTAGATCGAACTATTCGAACACTAAATA-tt-CAACTTAAC	Linear SABER for cone arrestin (Fig. 2 and Supplementary Fig. 3)
28*-t-28*-t-28*-ttt-p.25	GTTAAGTTG-t-GTTAAGTTG-t-GTTAAGTTG-ttt-CCAATAATA	Branched SABER for cone arrestin (Supplementary Fig. 3)
bc42_3*-tt-p.27-a-p.27	CTGTTGCGCGGGAGAACGACACGGACGCTAAATA TAGGAAAC-tt-CATCATCAT-a-CATCATCAT	SABER for SV2 - no amplification control (Supplementary Fig. 5)
bc42_3*-tt-p.27	CTGTTGCGCGGGAGAACGACACGGACGCTAAATA TAGGAAAC-tt-CATCATCAT	linear SABER for SV2 (Supplementary Fig. 5)
27*-t-27*-t-27*-ttt-p.28	ATGATGATG-t-ATGATGATG-t-ATGATGATG-ttt-CAACTTAAC	Branched SABER for SV2 (Supplementary Fig. 5)
28*-t-28*-t-28*-ttt-p.32	GTTAAGTTG-t-GTTAAGTTG-t-GTTAAGTTG-ttt-CTTTTTTC	Iterative SABER for SV2 (Supplementary Fig. 5)
bc42_2*-tt-p.25-a-p.25-a	GGAGAGGAATAGGATCGTACAGTGGATAAGGCG GCGATAACG-tt-CCAATAATA-a-CCAATAATA a	SABER for CD8a - unamplified control (Fig. 2 and Supplementary Fig. 3)
bc42_0*-tt-p.30-a-p.30-a	GGGTTATTGCGAGGATATAGGGCGTGGCGGTGTC ATAGAATT-tt-AATACTCTC-a-AATACTCTC a	SABER for Ki67 - unamplified control (Fig. 3 and Supplementary Fig. 5)
25mer-tester*-tt-a-p.27-a-p.27-a-p.28	CTAGATCGAACTATTCGAACACTAAATA-tt-a CATCATCAT-a-CATCATCAT-a-CAACTTAAC For 350-nt: 1 h reaction with 0.1 µM h.28.28.ip For 450-nt: 1 h reaction with 0.2 µM h.28.28.ip For 750-nt: 1 h reaction with 0.4 µM h.28.28.ip	Linear SABER for Lamin B - quantification strand (Supplementary Fig. 4)
28*-t-28*-t-28*-t-a-p.30-a-p.30-tt-p.25	GTTAAGTTG-t-GTTAAGTTG-t-GTTAAGTTG-t-a-AATACTCTC-a-AATACTCTC-tt-CCAATAATA For 250-nt: 1 h reaction with 0.05 µM h.25.25 For 450-nt: 1 h reaction with 0.15 µM h.25.25	Branched SABER for Lamin B - quantification strand (Supplementary Fig. 4)

Supplemental Notes

Supplemental Note 1. Antibody-DNA conjugations

Not all commercial antibodies are provided in a formulation readily available for conjugation (for example antibodies may be provided in unpurified whole serum form or formulated with stabilizers or protectors that interfere with conjugation). Hence customized formulation of antibodies may be required. In addition, we currently utilize non-specific conjugation to Lys residues and provide a simple protocol to prepare custom conjugation of antibodies (Agasti et al., Chem Sci, 2017; also see **Supplemental Protocols**). Although multiple DNA oligos can be attached to each antibody molecule for further signal amplification, our reaction conditions are optimized to achieve 1-3 oligos per antibody, to prioritize conserving the antigen recognition capability upon conjugation. Alternatively, site-specific conjugation chemistries could be utilized, including click labeling of antibody gylcosyl residues (available as the SiteClick™ kit from Thermo Fisher). Independent of the conjugation method, we recommend testing of antibodies after conjugation to ensure functionality through comparison of the staining pattern with unconjugated antibody. As the high potential of DNA barcoding gains higher recognition and visibility, commercial antibody-DNA conjugation services and ready-to-use kits are also becoming available. Additionally, alternative recent probes (recombinant antibodies, nanobodies, aptamers, etc.) and probe labeling methods (such as unnatural amino acid incorporation or engineering of site-specific adaptor molecules) could facilitate new and highly-efficient means for standardized large-scale probe libraries as future resources.

Ref: Agasti, S.S., Wang, Y., Schueder, F., Sukumar, A., Jungmann, R., & Yin, P. DNA-barcoded labeling probes for highly multiplexed Exchange-PAINT imaging. *Chemical Science*, *8*(4), 3080-3091 (2017).

Supplemental Note 2. Sample stability over time

A potentially important factor for reproducibility is the time between sample preparation and imaging. To enable easy washing for multiplexing, the imager binding is designed to be not extremely stable. When samples are kept in buffer (such as PBS) over extended periods, imagers might get lost over time. To avoid that, we recommend paying attention to this factor in experimental design, and either keeping the storage conditions and time similar in between experiments (for exchange imaging), or to use curing embedding media (such as ProLong Diamond) to keep the imagers from de-hybridizing and diffusing away (for spectral multiplexing without exchange) (also see **Supplemental Protocols – General recommendations**).

Supplemental Note 3: Tensorflow implementation hyperparameters for nuclear segmentation

We used our own implementation in TensorFlow with the following hyperparameters: Number of feature maps in first convolutional layer: 8; Number of feature maps in subsequent downsampling layers: 2 times the number of feature maps in previous layer; Downsampling and upsampling factor: 2; Convolution kernel size: 3; Number of extra convolutions in each layer: 1; Variance of truncated normal distribution generating initial random weights: 0.1; Number of downsampling layers: 2; Batch size: 8; Number of training steps: 20,000; Learning rate: initially 0.1, with 'staircase' exponential decay (step 1000, rate 0.95), and momentum 0.9.